

***2. Karbonáty I. –
mineralogie, komponenty,
struktury, sedimentační
prostředí***

Karel Martínek

Ústav geologie a paleontologie

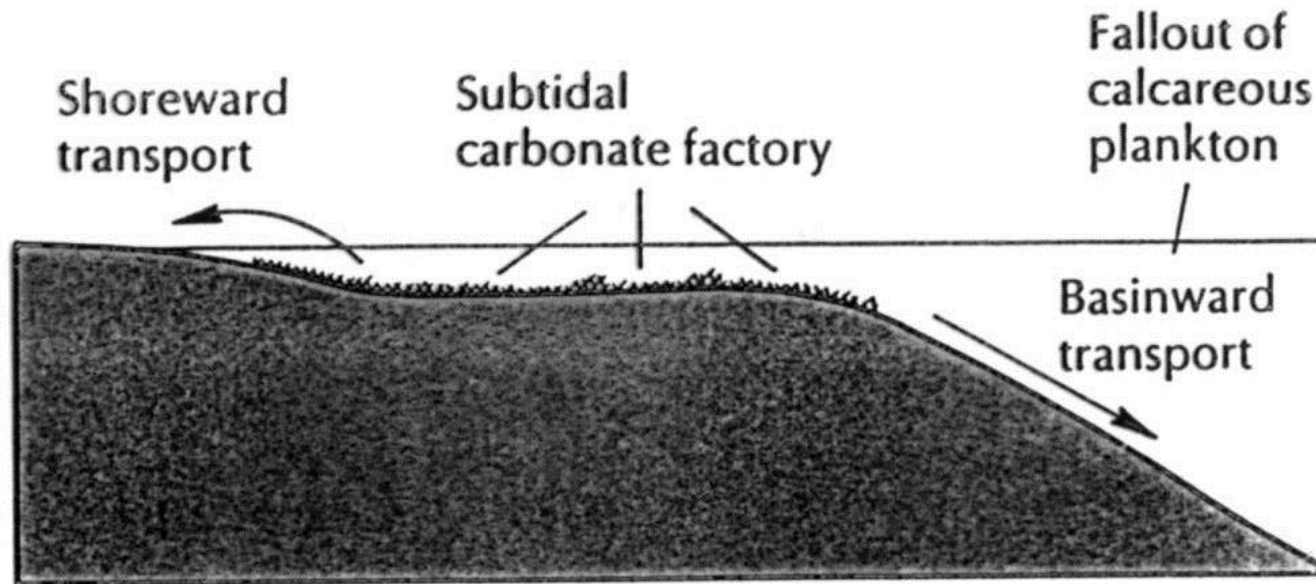


Figure 6.1

Sketch of carbonate shelf, showing main regions of accumulation of carbonate sediments. From James (1984).

Table 6.1

Differences between Siliciclastic and Carbonate Sediments

Carbonate Sediments	Siliciclastic Sediments
Most sediments occur in shallow, tropical environments.	Climate is no constraint, so sediments occur worldwide and at all depths.
Most sediments are marine.	Sediments are both terrestrial and marine.
The grain size of sediments generally reflects the size of organism skeletons and calcified hard parts.	The grain size of sediments reflects the hydraulic energy in the environment
The presence of lime mud often indicates the prolific growth of organisms whose calcified portions are mud-sized crystallites.	The presence of mud indicates settling out from suspension.
Shallow-water lime sand bodies result primarily from localized physico-chemical or biological fixation of carbonate.	Shallow-water sand bodies result from the interaction of currents and waves.

Localized buildups of sediments without accompanying change in hydraulic regimen alter the character of surrounding sedimentary environments.

Sediments are commonly cemented on the seafloor.

Periodic exposure of sediments during deposition results in intensive diagenesis, especially cementation and recrystallization.

The signature of various sedimentary facies is obliterated during low-grade metamorphism.

Changes in the sedimentary environments are generally brought about by widespread changes in the hydraulic regimen.

Sediments remain unconsolidated in the environment of deposition and on the seafloor.

Periodic exposure of sediments during deposition leaves deposits relatively unaffected.

The signature of sedimentary facies survives low-grade metamorphism.

From James (1984).

mineralogie

kalzit (low Mg, high Mg), aragonit, dolomit

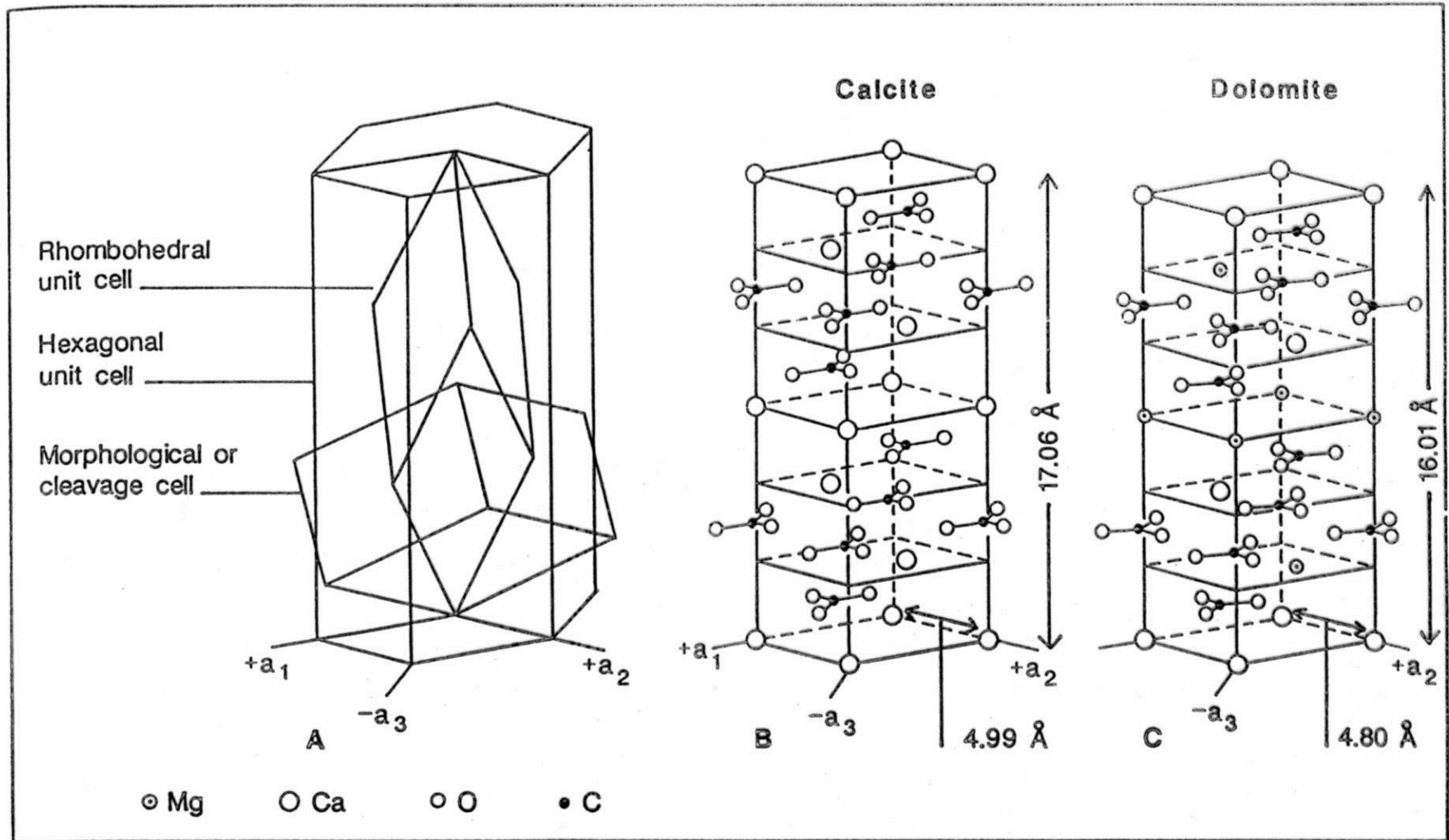
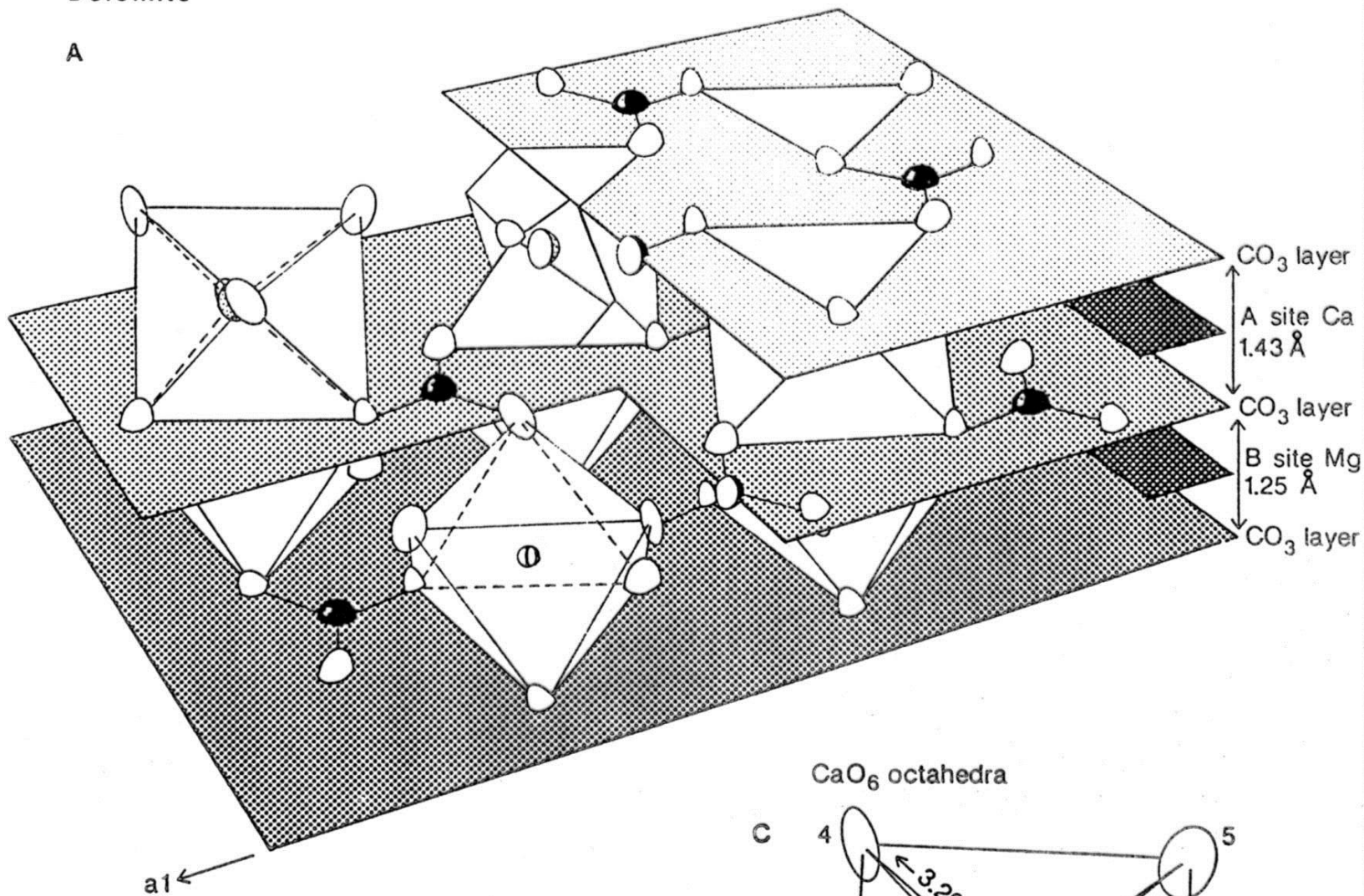


Fig. 6.1 (A) Diagrammatic relationship between rhombohedral, hexagonal and morphological unit cells and the hexagonal crystallographic axes. (B) Hexagonal unit cell of calcite, apparent rectilinear shape due to perspective; a_1 , a_2 and $a_3 = 4.99 \text{ \AA}$; $c = 17.06 \text{ \AA}$. (C) Hexagonal unit cell of dolomite; a_1 , a_2 and $a_3 = 4.80 \text{ \AA}$; $c = 16.01 \text{ \AA}$.

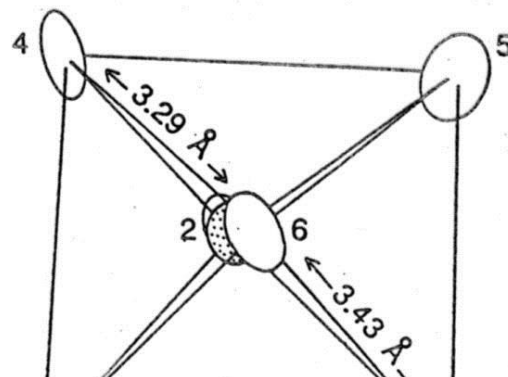
Dolomite

A



CaO_6 octahedra

C



B



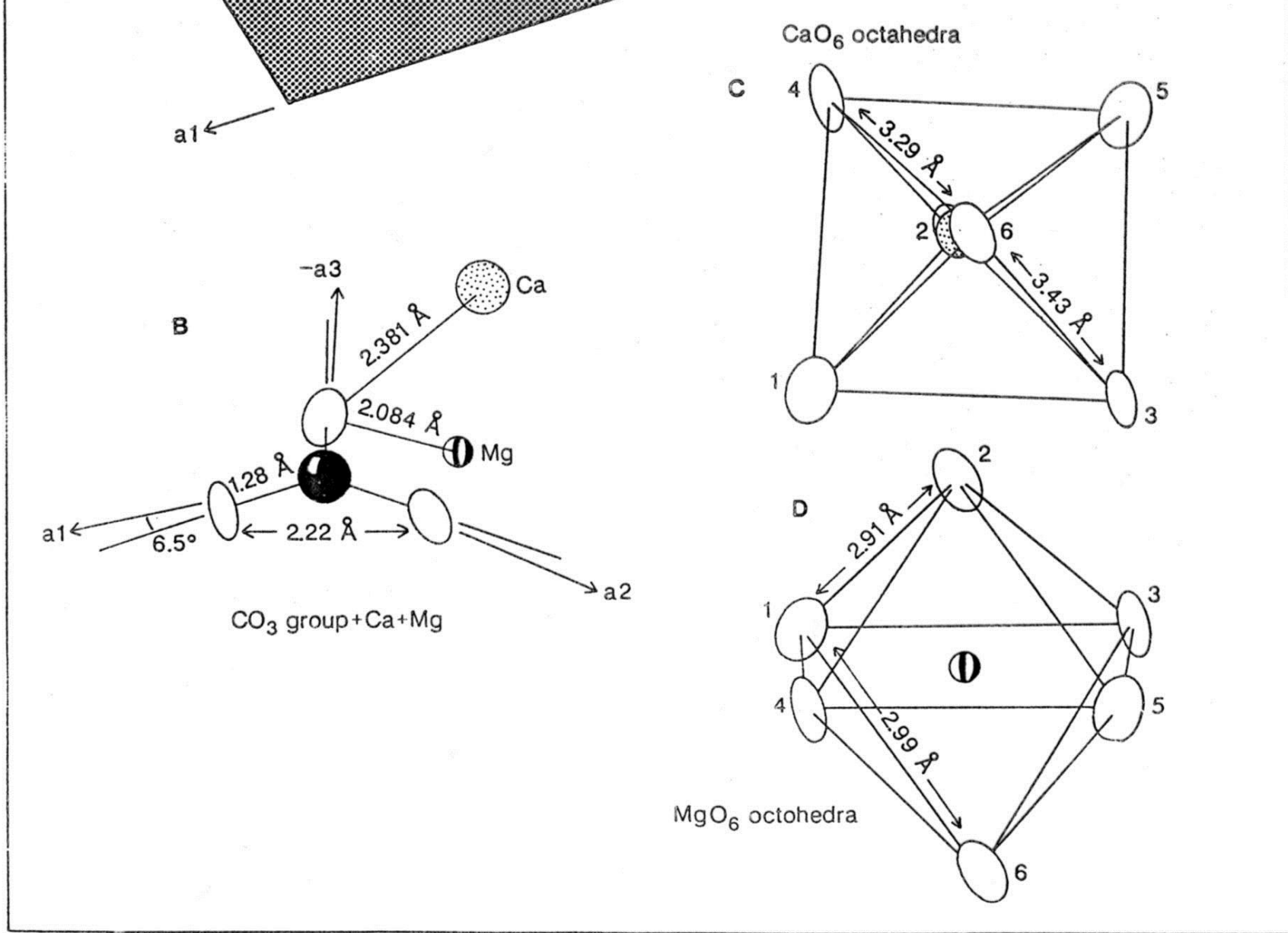
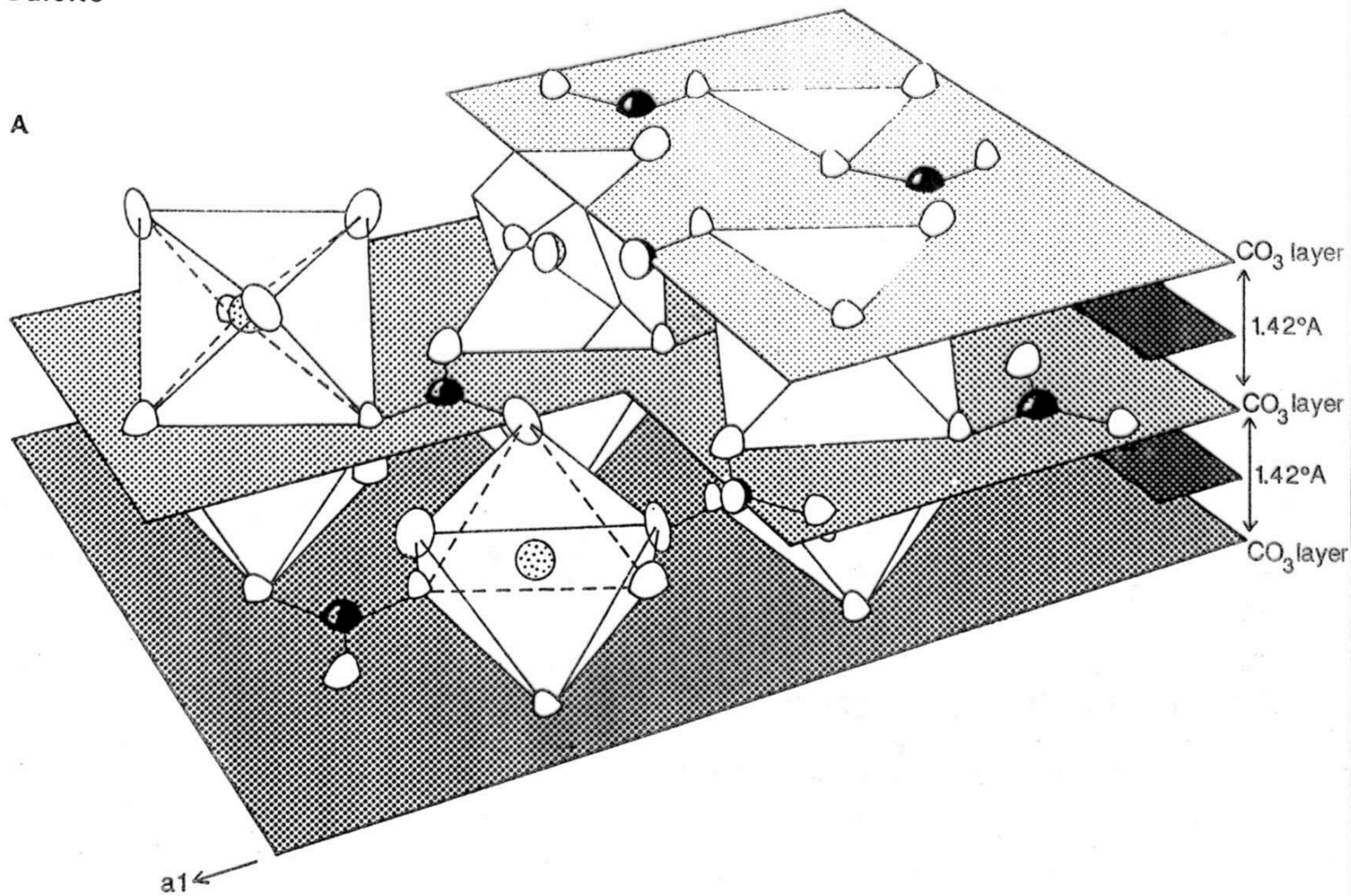


Fig. 6.3 (A) Perspective view of portion of dolomite lattice, symbols as for Fig. 6.2 with vertically striped spheres = magnesium ions. Note rotation of structural units relative to a_1 direction and different layer thicknesses compared to Fig. 6.2. (B) CO_3 group. Note 6.5° rotation of C–O bonds relative to a_1 axis. (C) CaO_6 and (D) MgO_6 octahedral bonding.

Calcite

A



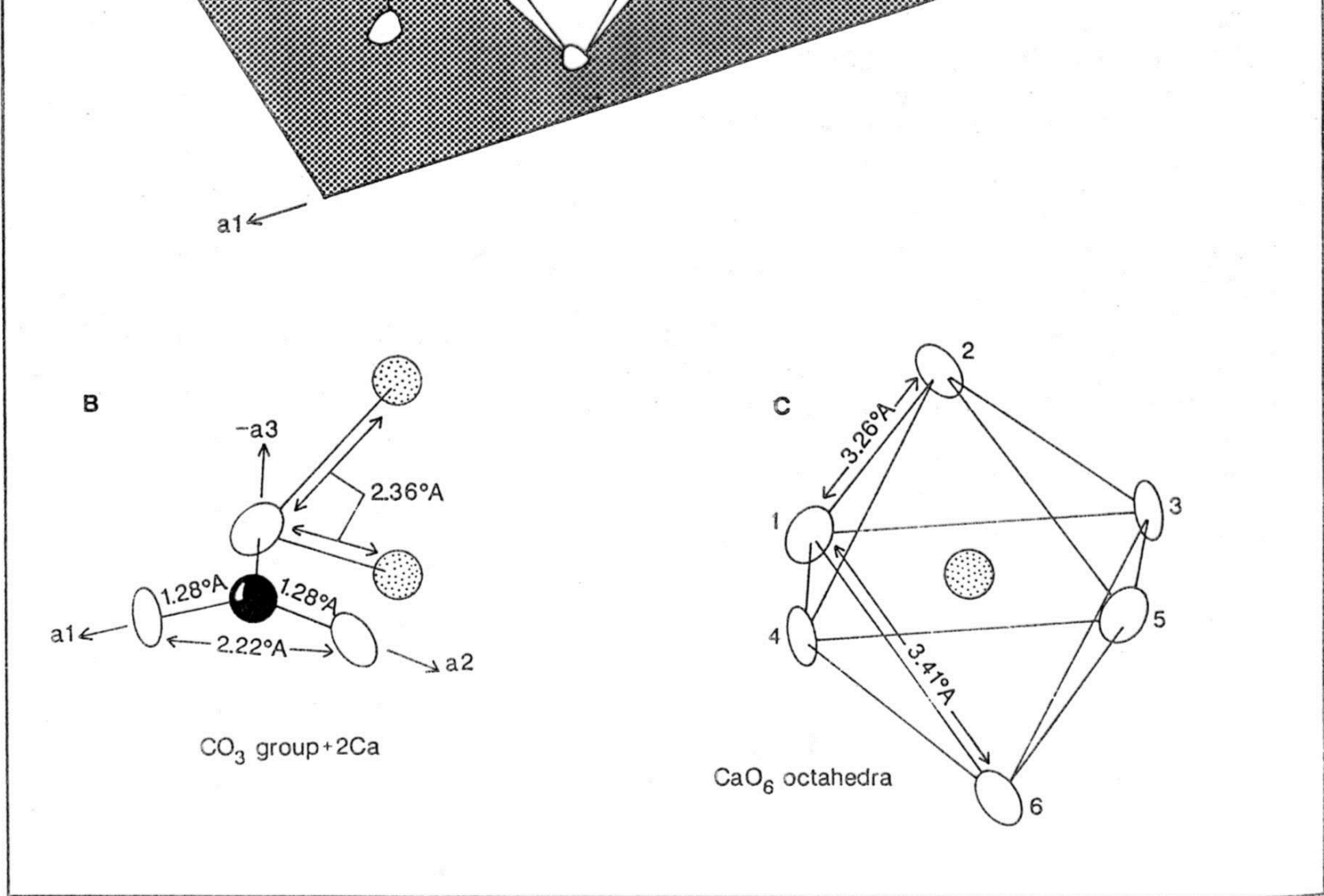


Fig. 6.2 (A) Perspective view of portion of calcite lattice in which the layered nature is emphasized by shaded planes: black spheres = carbon atoms stippled spheres = calcium atoms and unshaded ellipsoids = oxygen atoms. CO_3 groups intersected by three full planes. Position of Ca planes shown by partial planes at right margin. CaO_6 octahedra between CO_3 layers unshaded. (B) CO_3 group with one oxygen showing two bonded Ca ions. (C) CaO_6 octahedron showing bond lengths.

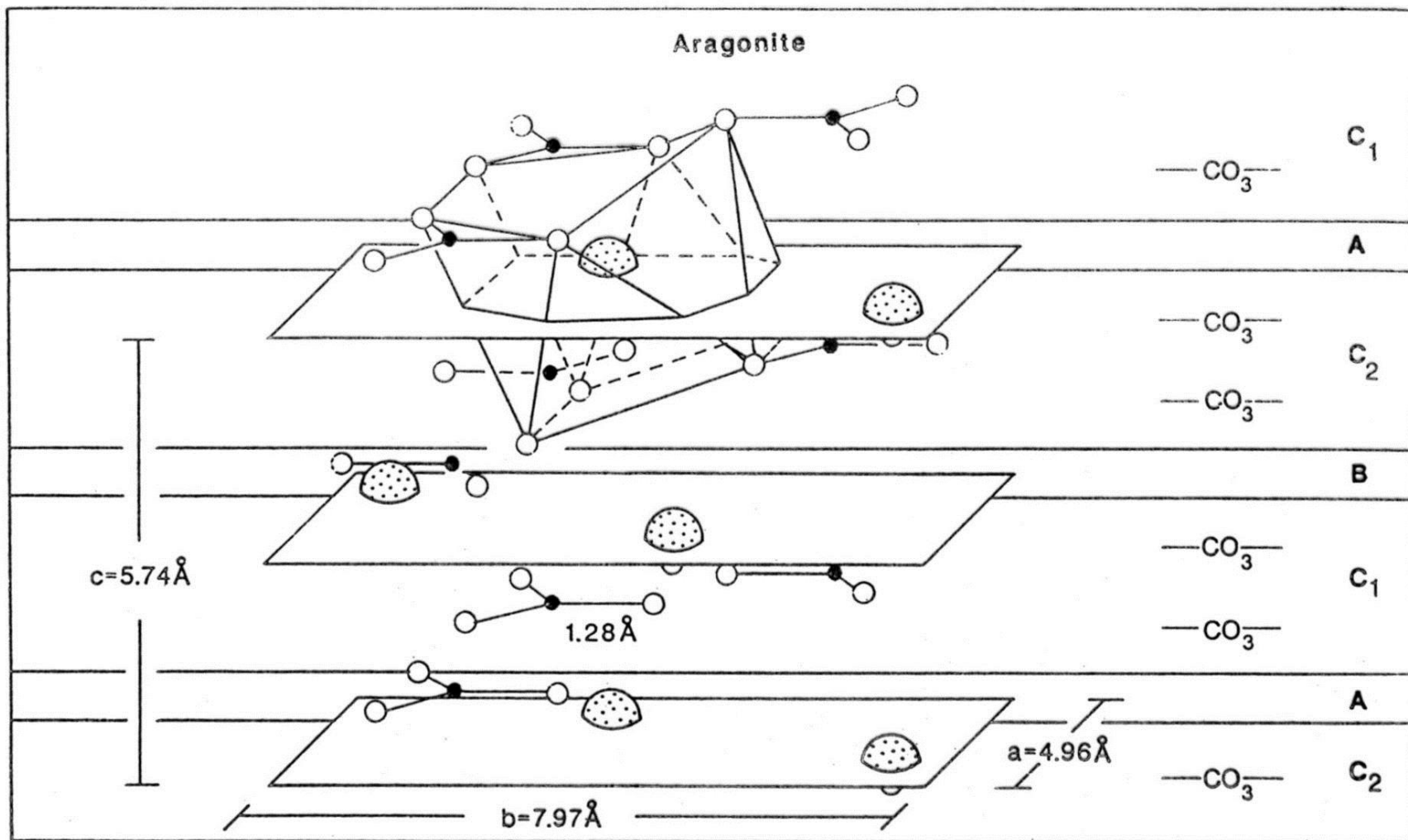


Fig. 6.4 Projection emphasizing the layered nature of the aragonite structure against a (100) plane. Three unshaded horizontal planes intersecting stippled calcium atoms (ABAB layering). Black spheres = carbon atoms, unshaded spheres = oxygen atoms. The CaO₉ co-ordination polyhedron characteristic of the orthorhombic carbonates outlined. Unit cell dimensions shown.

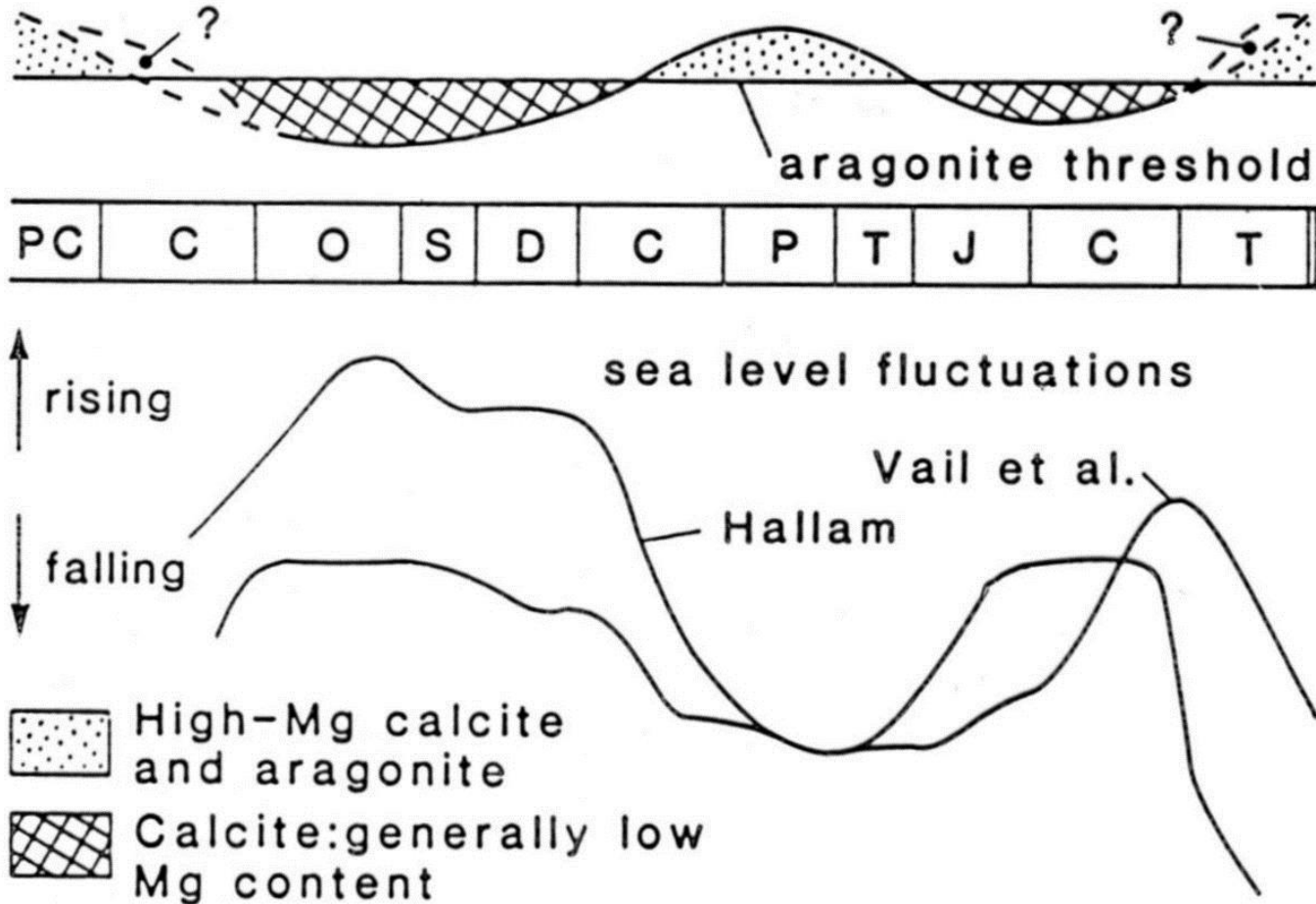


Fig. 4.4 Mineralogy of marine, abiogenic, carbonate precipitates through the Phanerozoic, compared with the global sea-level curve. After Sinberg (1983).

komponenty

ooidy, pisoidy, peloidy, agregáty, intraklasty, bioklasty, řasy, stromatolity, karbonátový kal, Folkova klasifikace (1962)

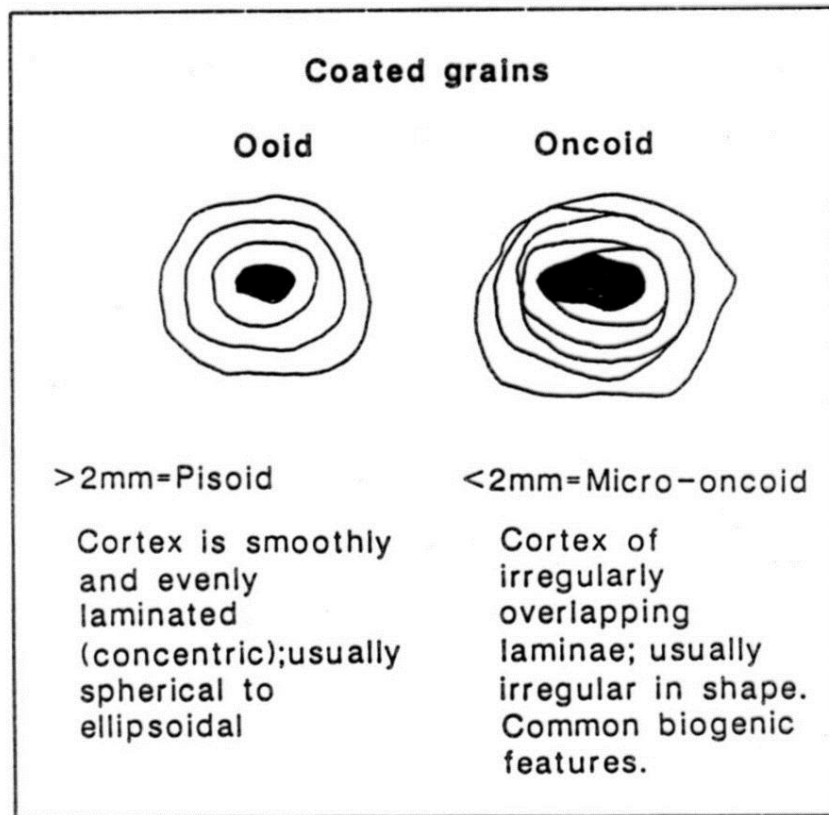


Fig. 1.1 Classification of coated grains.

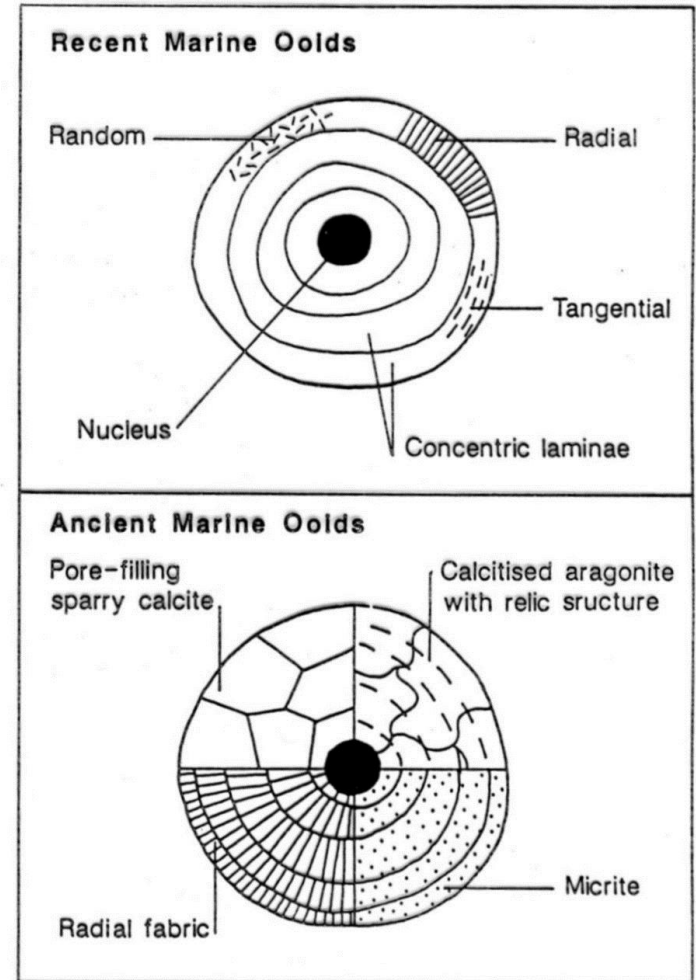
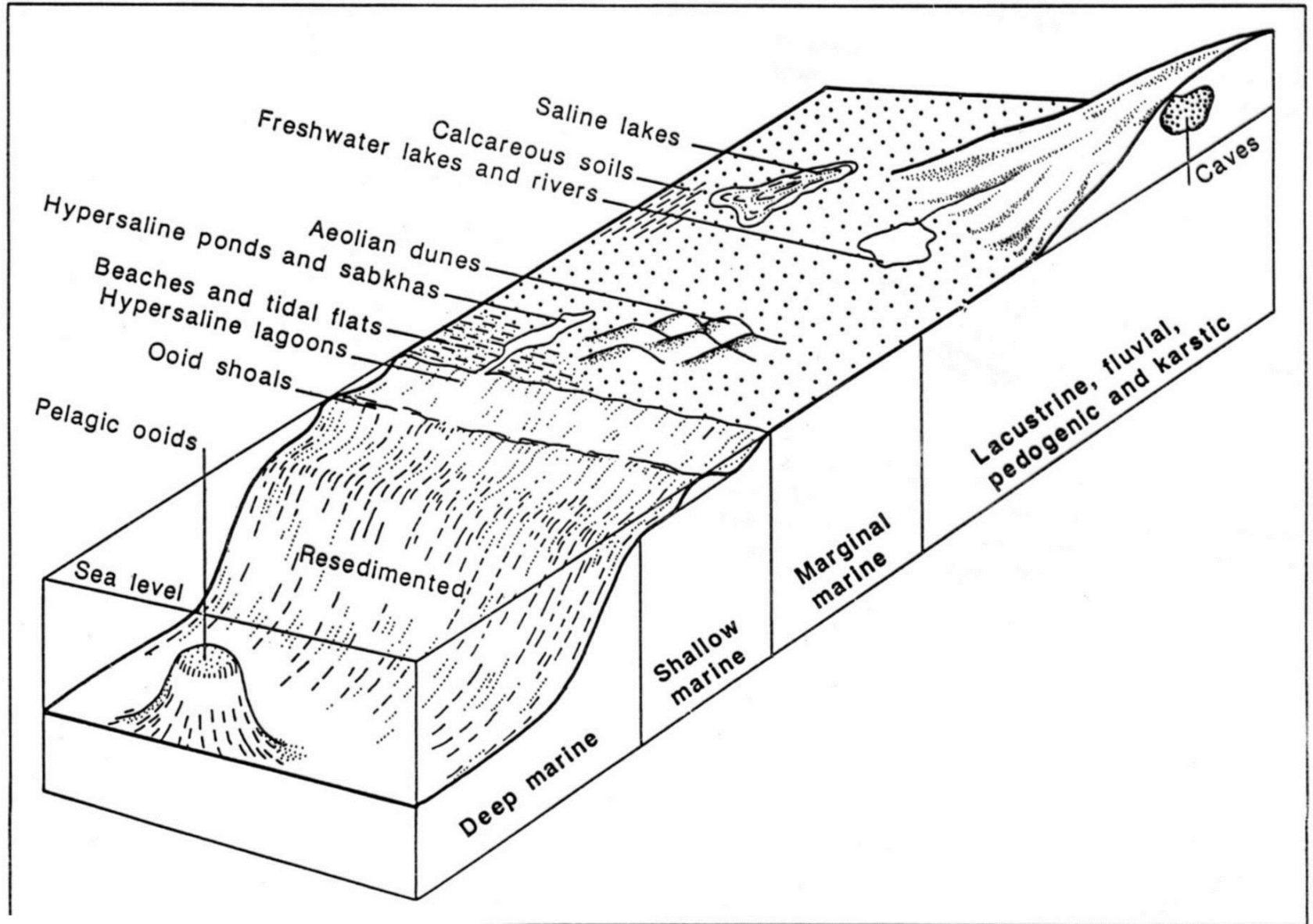


Fig. 1.2 Major types of microstructure seen in modern and ancient ooids. Variations on these types have been described from ancient ooids by Tucker (1984), Strasser (1986), Chow & James (1987) and Singh (1987).

Fig. 1.4 Sites of formation and deposition of coated grains.



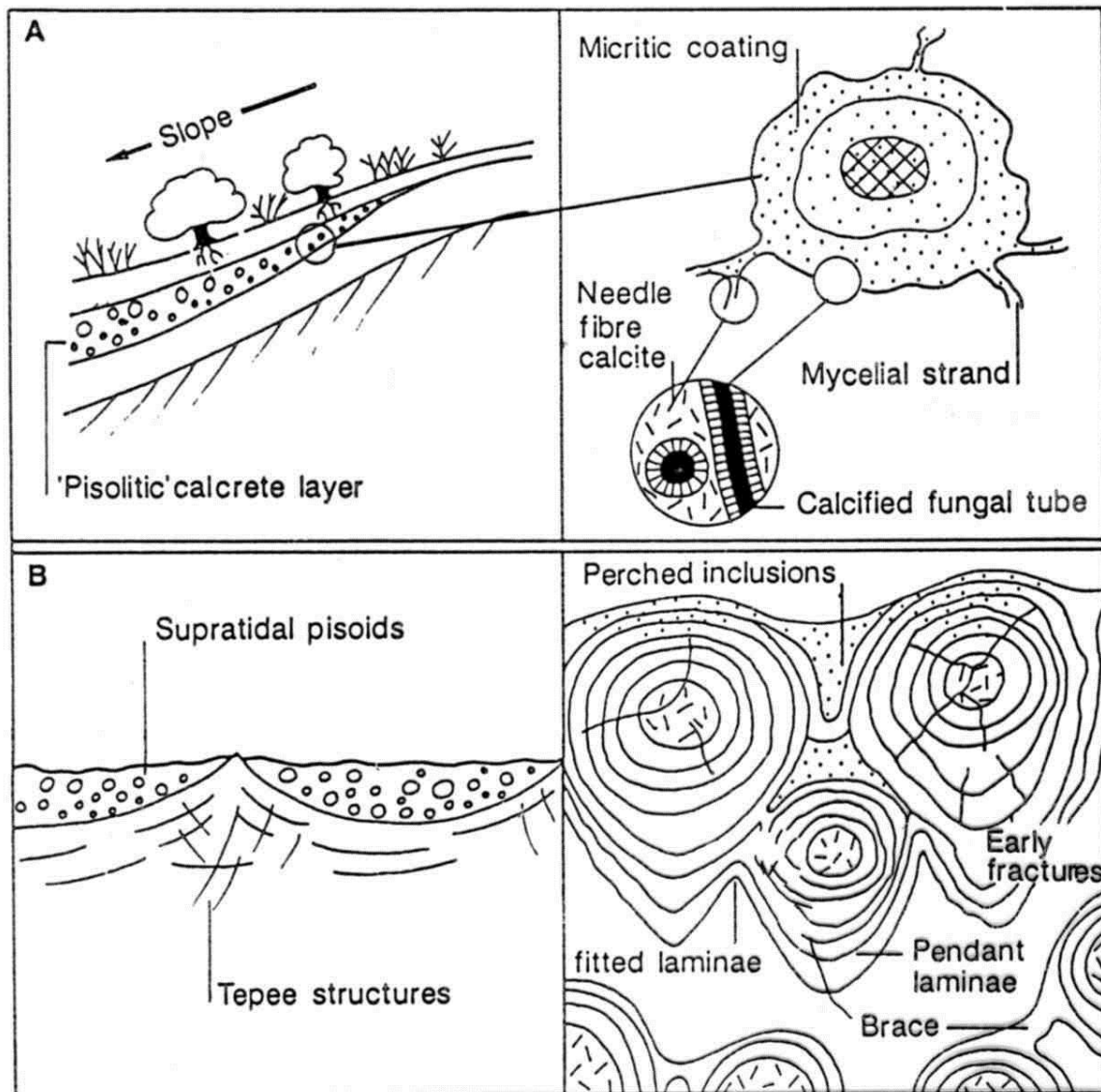


Fig. 1.5 Vadose and calcrete-coated grains. (A) Calcrete profile with coated grain horizon related to soil creep. The coatings are commonly non-isopachous and may have calcified outgrowths of mycelial bundles. Internally the micritic laminae exhibit a variety of microbial tubes and acicular calcites (e.g. Calvet & Julia, 1983). (B) Supratidal vadose pisoids commonly formed within tepee pools (e.g. Esteban & Pray, 1983). During the early stages of growth the pisoids were free to rotate and have isopachous coatings. In the later stages they were immobile and the coatings exhibit downward (pendant) forms and are 'fitted' (laminae shared by adjacent pisoids). Other features indicating static growth include perched inclusions and braces. Desiccation, it seems, results in early fracturing.

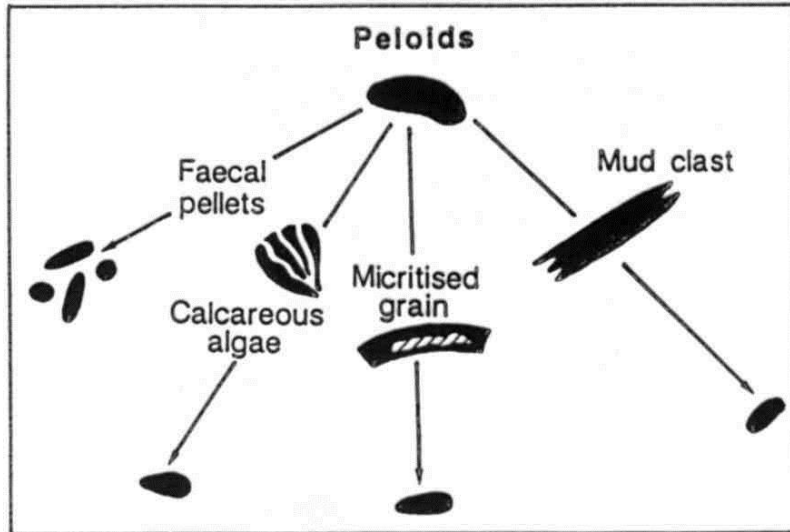


Fig. 1.7 *Origins of peloids.*

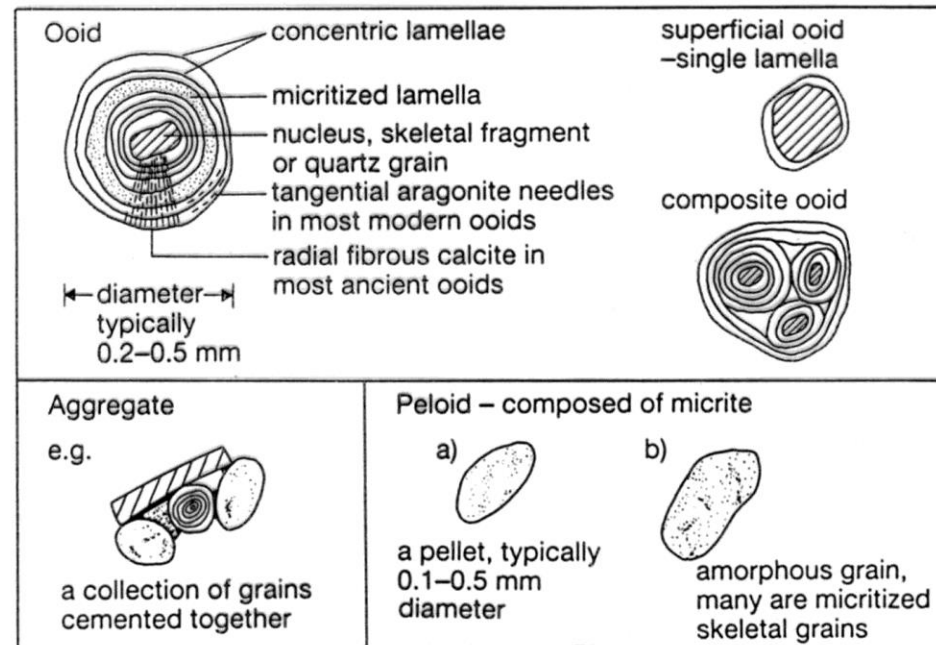


Fig. 4.1 The principal non-skeletal grains in limestones: ooids, peloids and aggregates.

Table 4.1 The mineralogy of carbonate skeletons (x = dominant mineralogy, (x) = less common). During diagenesis, these mineralogies may be altered or replaced; in particular, aragonite is metastable and is invariably replaced by calcite, and high-Mg calcite loses its Mg

Organism	Mineralogy			
	Aragonite	Low-Mg calcite	High-Mg calcite	Aragonite + calcite
Mollusca:				
bivalves	x	x		x
gastropods	x			x
pteropods	x			
cephalopods	x		(x)	
Brachiopods		x	(x)	
Corals:				
scleractinian	x			
rugose + tabulate		x	x	
Sponges	x	x	x	
Bryozoans	x		x	x
Echinoderms			x	
Ostracods		x	x	
Foraminifera:				
benthic	(x)		x	
pelagic		x		
Algae:				
coccolithophoridae		x		
rhodophyta	x		x	
chlorophyta	x			
charophyta		x		

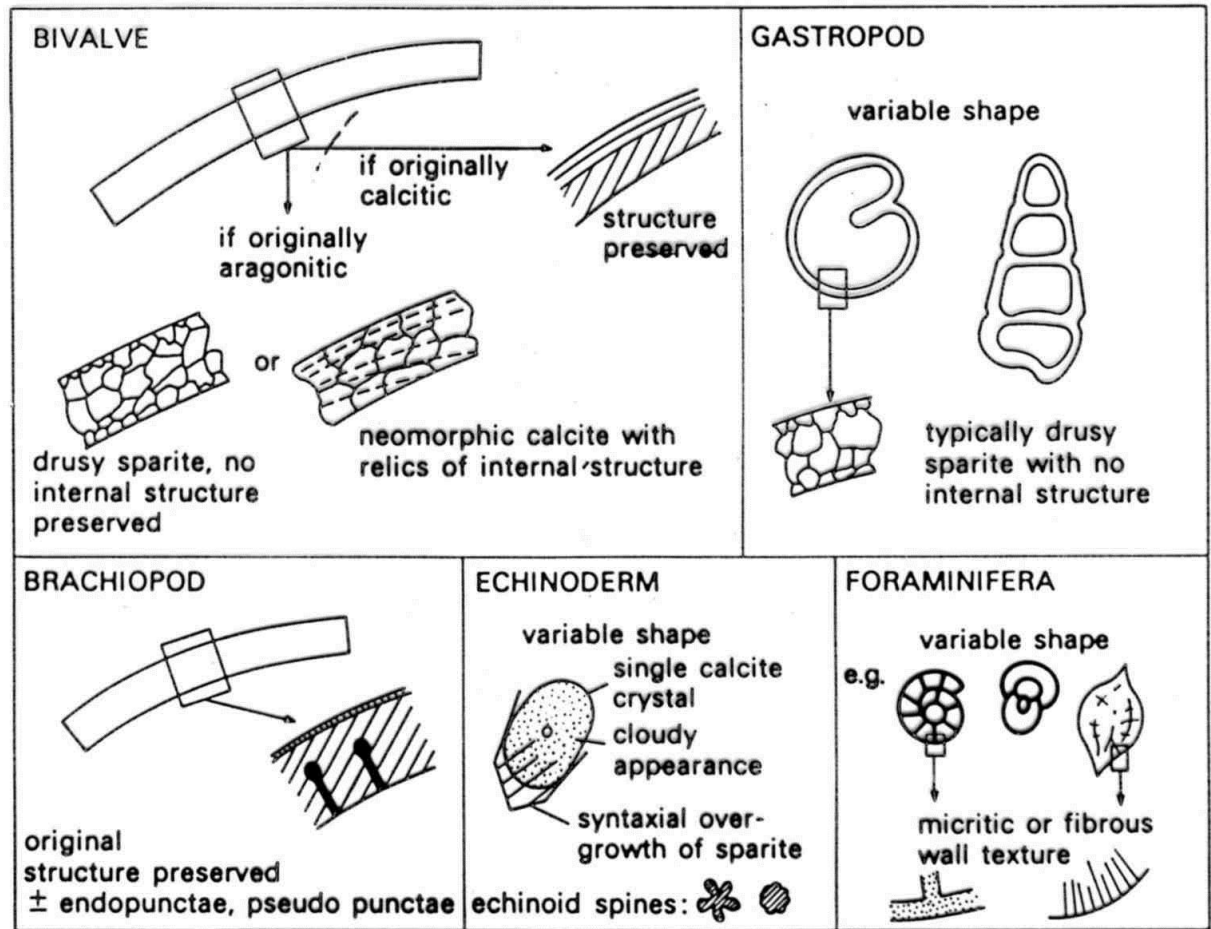


Fig. 4.9 Typical thin-section appearance of bivalve, gastropod, brachiopod, echinoderm and foraminiferal skeletal grains in limestone.

studium ultrastruktur – pro lepší identifikaci organismů

Molluscan aragonite shell replacement

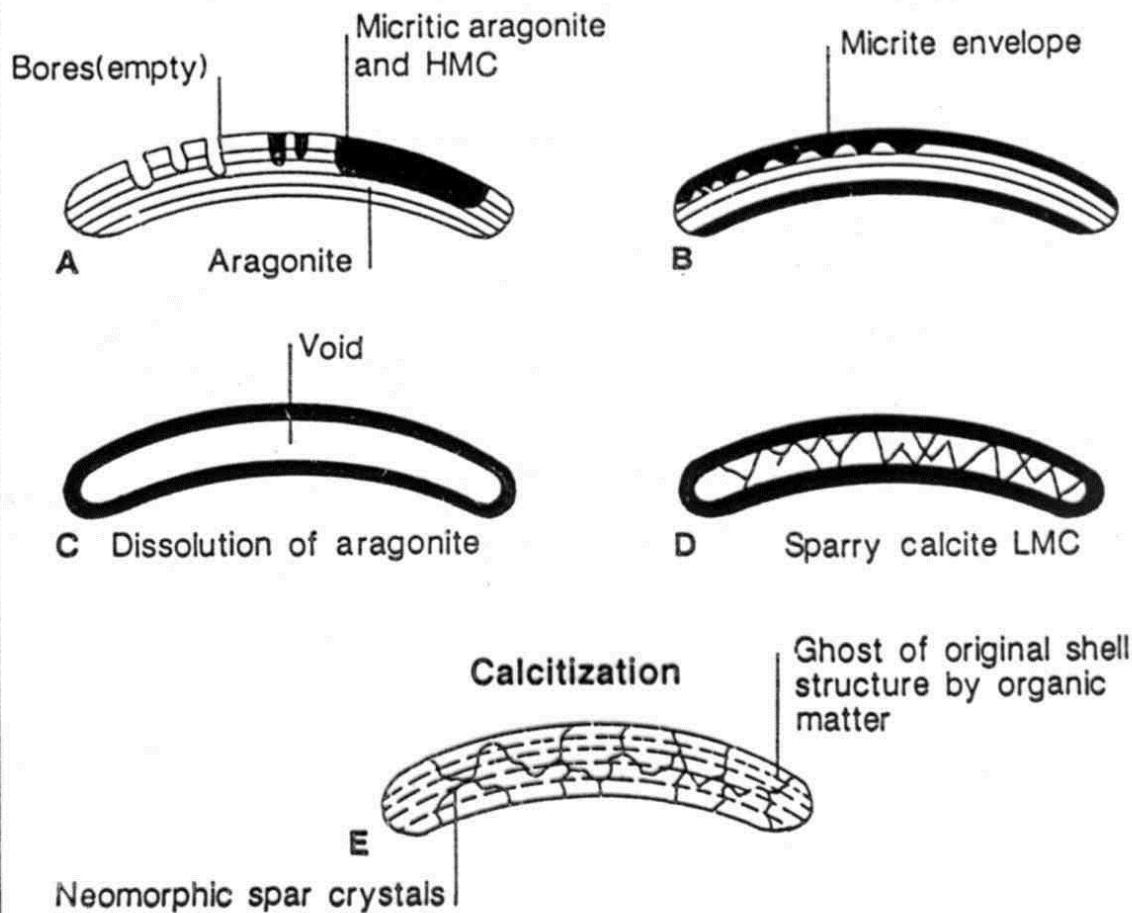


Fig. 1.10 Molluscan aragonite shell replacement. (A–D) By a dissolution–cementation process. (E) By calcitization with the preservation of relic microarchitecture (see text and Section 7.2).

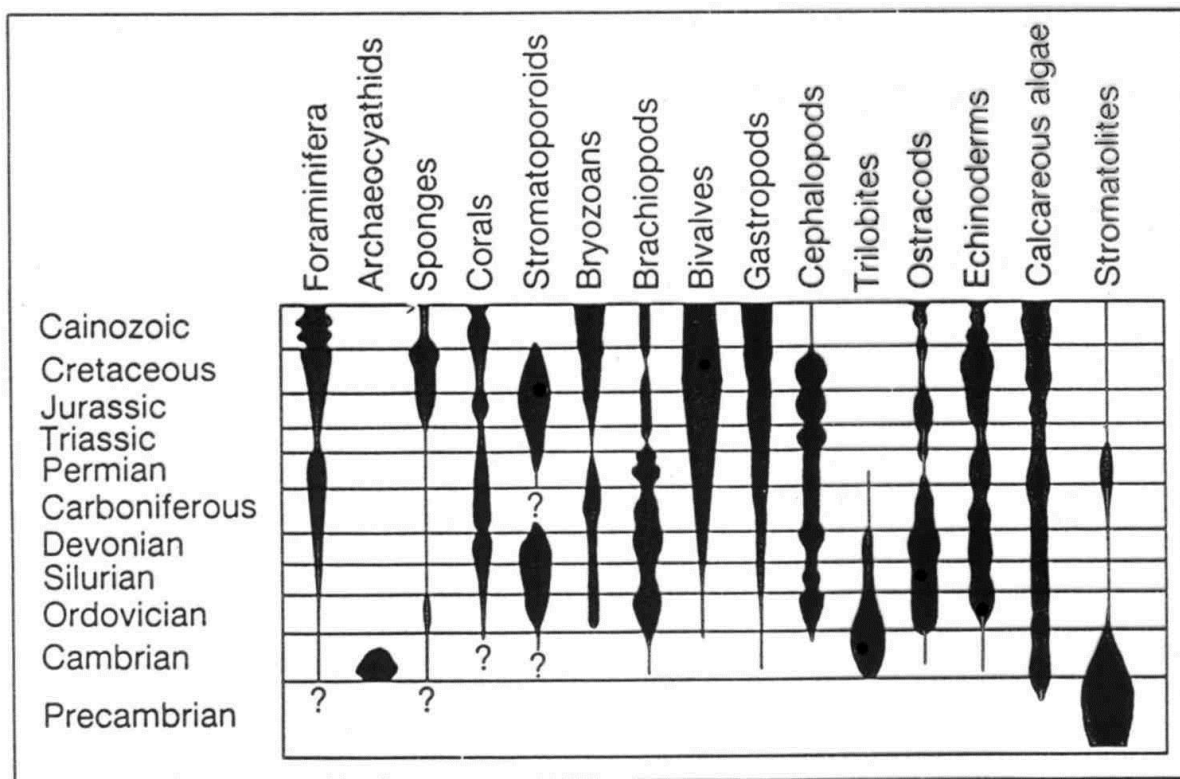


Fig. 4.7 Age range and generalized taxonomic diversity of principal carbonate-secreting organisms. After Horowitz & Potter (1971).

biomineralizace

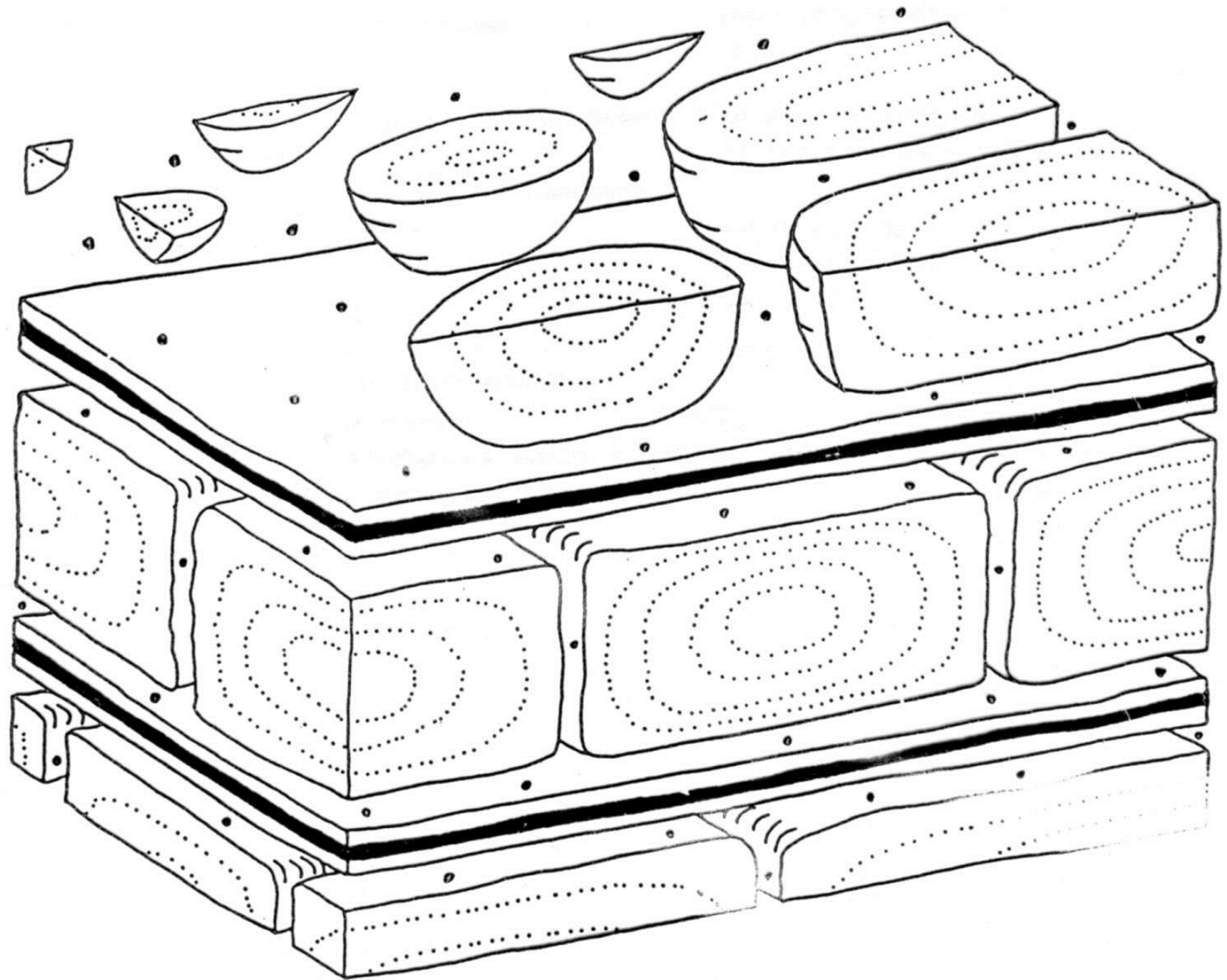
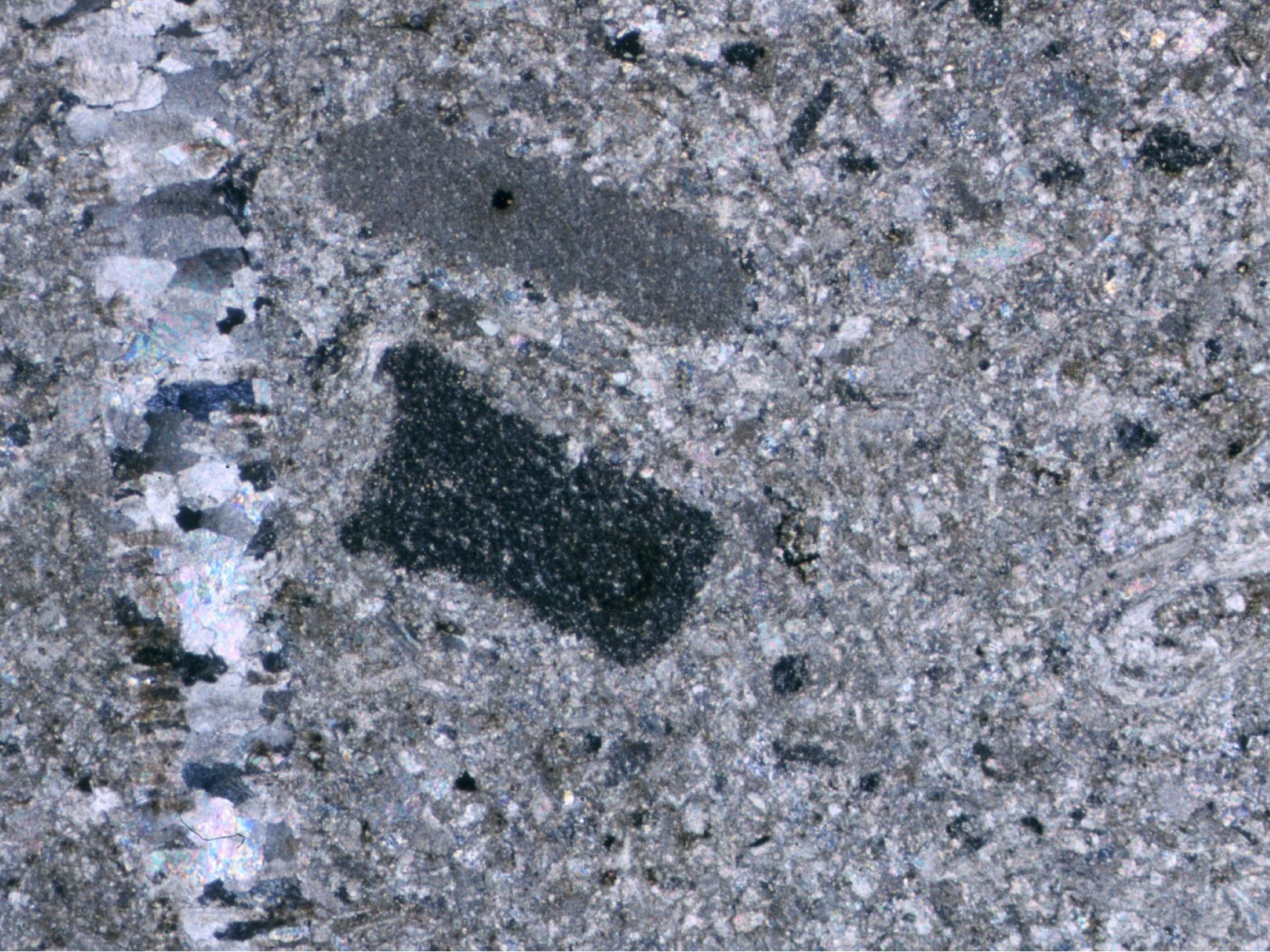


Fig. 6.9 Diagrammatic example of molluscan biomineralization. The central layer and lower half layer are completely mineralized by aragonite single crystal tablets (shown with growth rings). The upper half layer is undergoing mineralization, the aragonite crystals being seeded in a layer composed of acidic amino acids (large dots). The black layer (B-chitin) and unshaded layers (silk, fibroin-like proteins) separate the mineralizing layers. After Weiner & Traub (1984).



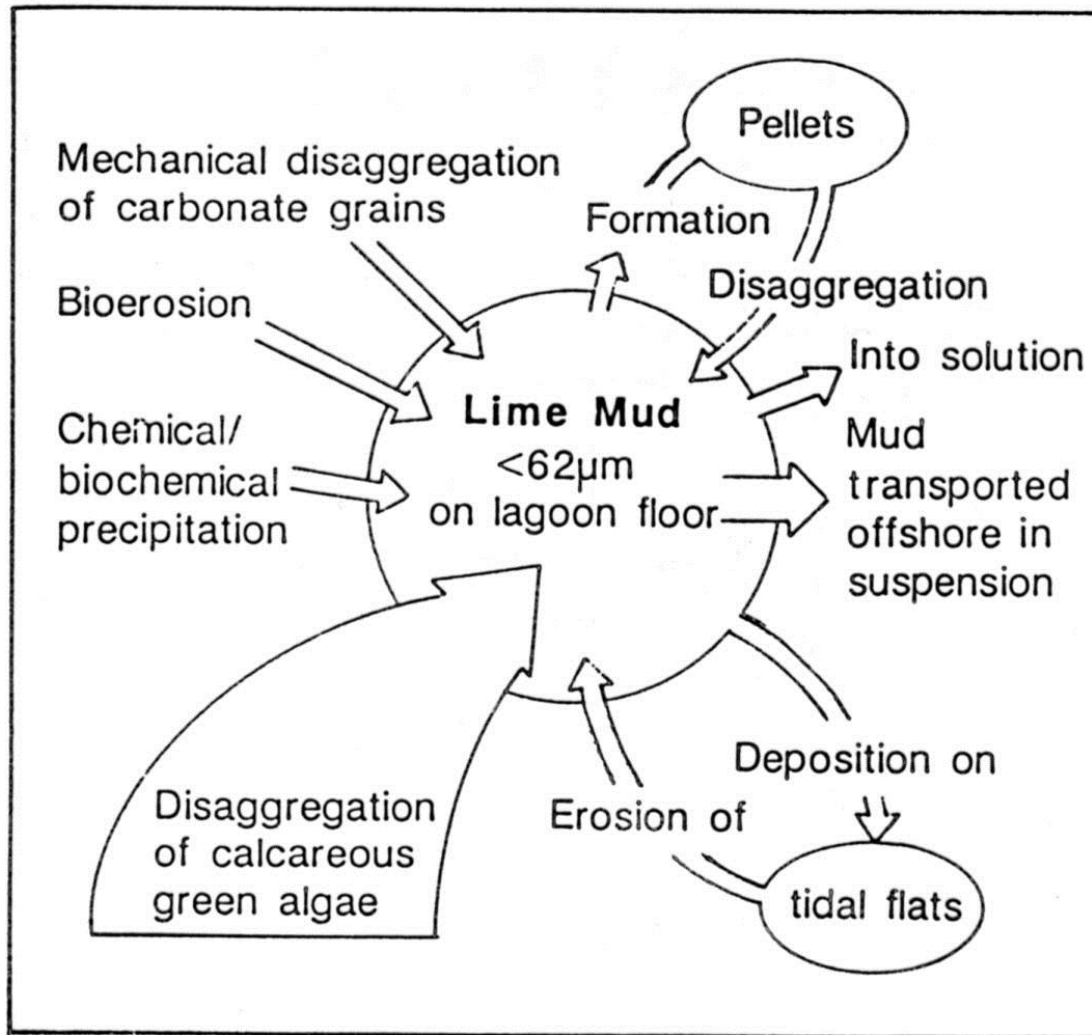


Fig. 1.13 *Lime mud budget for the Bight of Abaco, Bahamas. Based on Neumann & Land (1975) and Tucker (1981).*





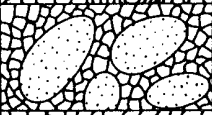




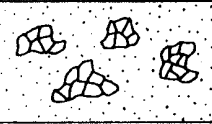
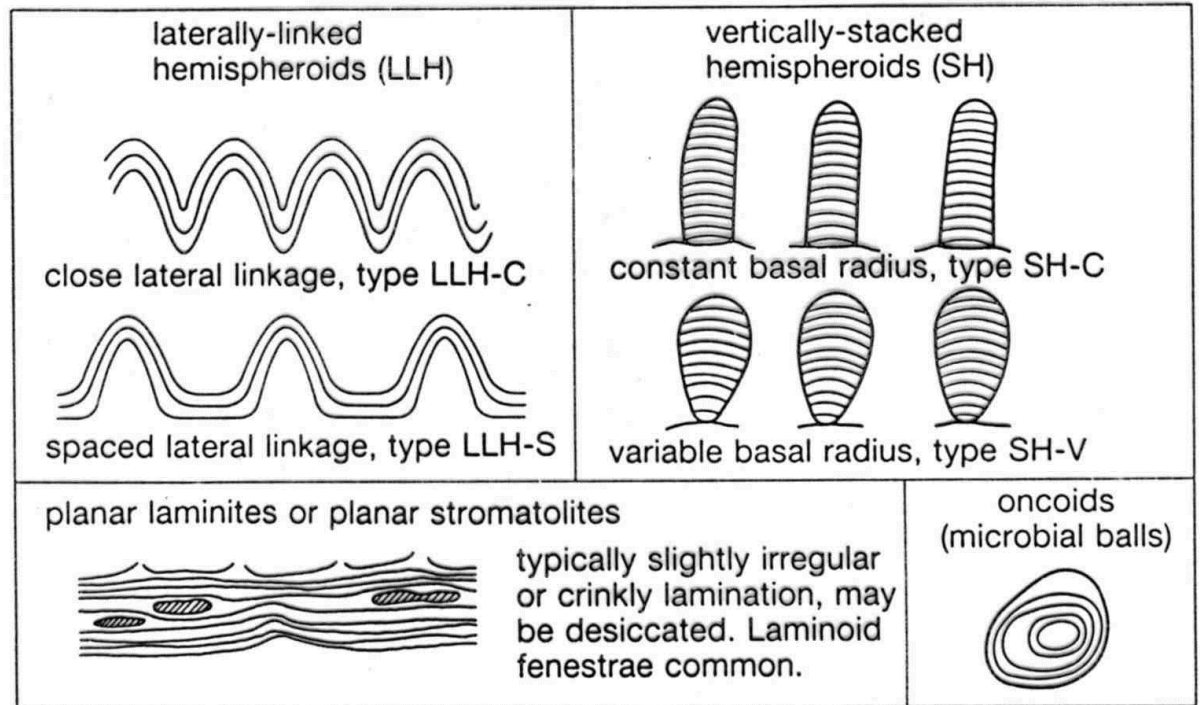
Principal allochems in limestone	Limestone types			
	cemented by sparite		with a micritic matrix	
skeletal grains (bioclasts)	biosparite		biomicrite	
ooids	oosparite		oomicrite	
peloids	pelsparite		pelmicrite	
intraclasts	intrasparite		intramicrite	
limestone formed in situ	biolithite		fenestral limestone -dismicrite	

Fig. 4.35 Classification of limestones based on composition. After Folk (1962).

Fig. 4.31 Common types of stromatolite with terminology. After Logan *et al.* (1964).



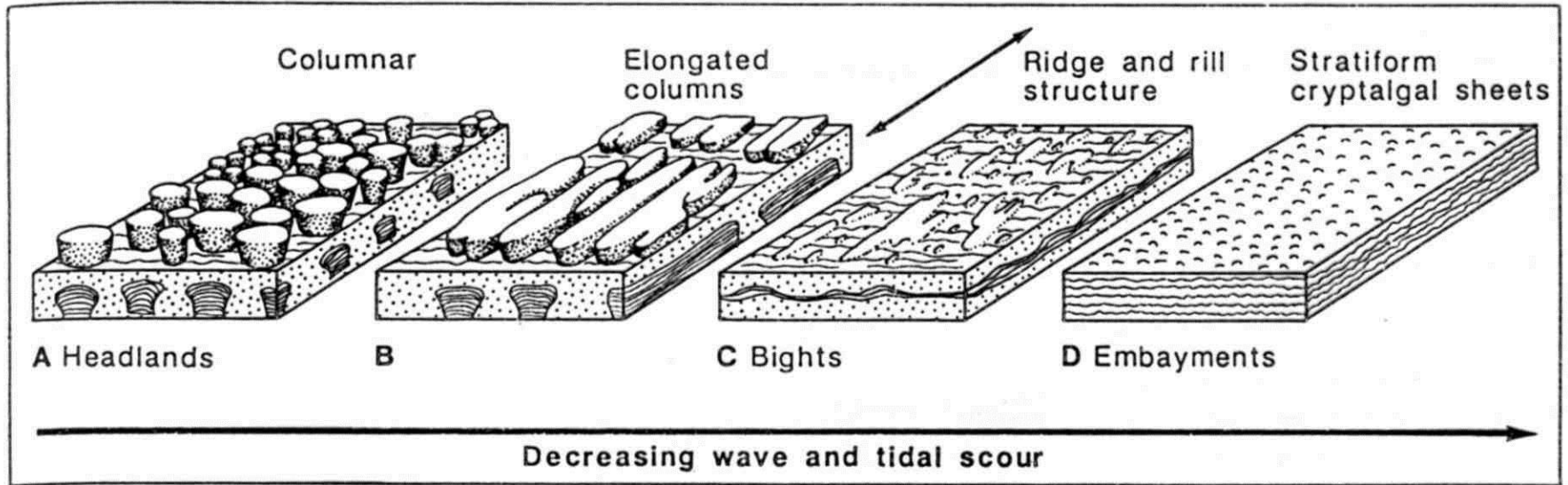


Fig. 4.49 Schematic diagram of the variations in stromatolite form related to wave and tidal scour (modified from Wright, 1984). Discrete columnar forms (A) occur on headlands fully exposed to waves. The relief of the columns is proportional to the intensity of wave action. Elongation of the columns occurs parallel to the direction of wave attack (B) and occurs in less-exposed bights near headlands. In areas partially protected from wave attack, ridge and rill structures develop (C) with relief of 0.1–0.3 m. In small embayments, completely protected from waves, stratiform sheets occur with relief of less than 40 mm (D). These four all represent pustular mat forms from Shark Bay. Based on data in Hoffman (1976). However, Burne & James (1986) have interpreted the intertidal columnar forms as subtidal forms exposed by a drop in sea-level. Similar subtidal forms have been described from tidal channels in the Bahamas by Dill et al. (1986; Fig. 3.12).

struktury

teepee, hardgroundy, ptačí oči (birdseyes), paleokras, strukturní klasifikace (Dunham 1962)


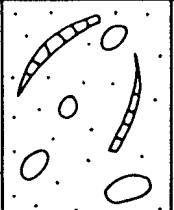
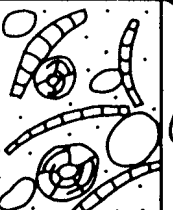
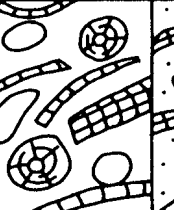







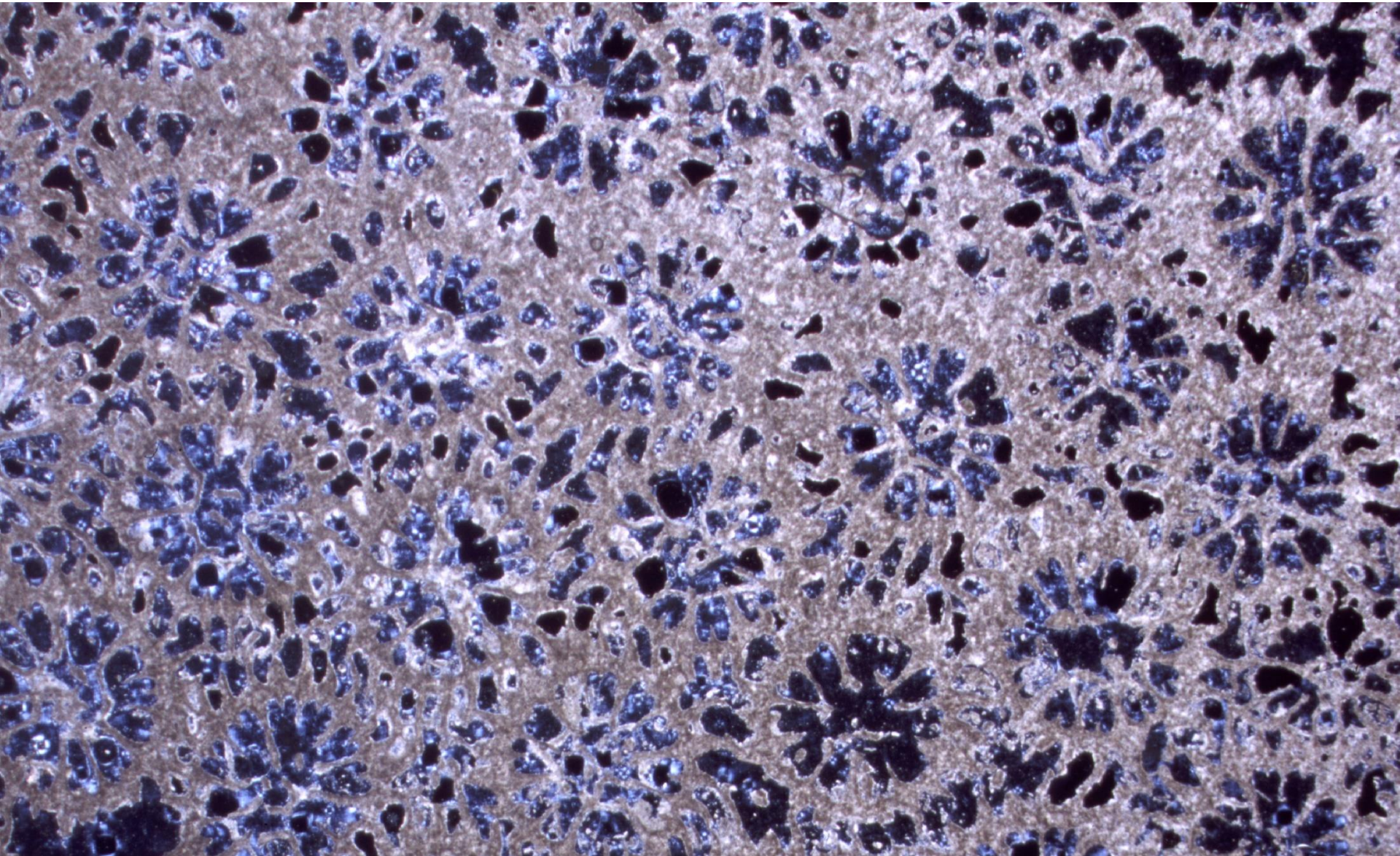
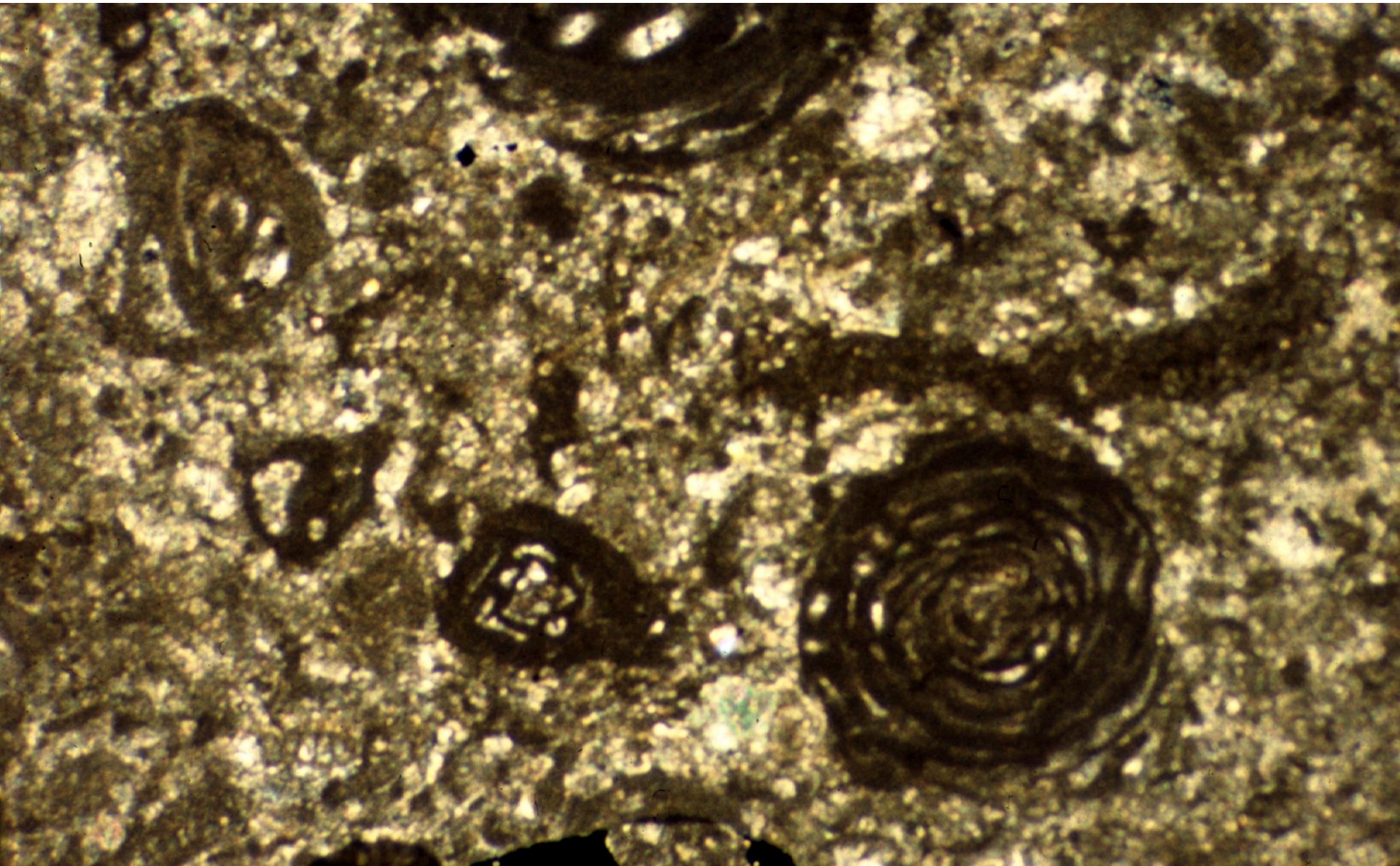
original components not bound together during deposition		lacks mud and is grain supported	original components bound together	depositional texture not recognizable	crystalline carbonate	original components not organically bound during deposition		original components organically bound during deposition		
contains lime mud						>10% grains >2mm				
mud-supported		grain-supported				matrix supported	supported by > 2mm component	organisms act as baffles	organisms encrust and bind	organisms build a rigid framework
less than 10% grains	more than 10% grains									
mudstone	wackest.	packstone	grainstone	bound stone	crystalline	floatstone	rudstone	baffle stone	bindstone	frame stone
										

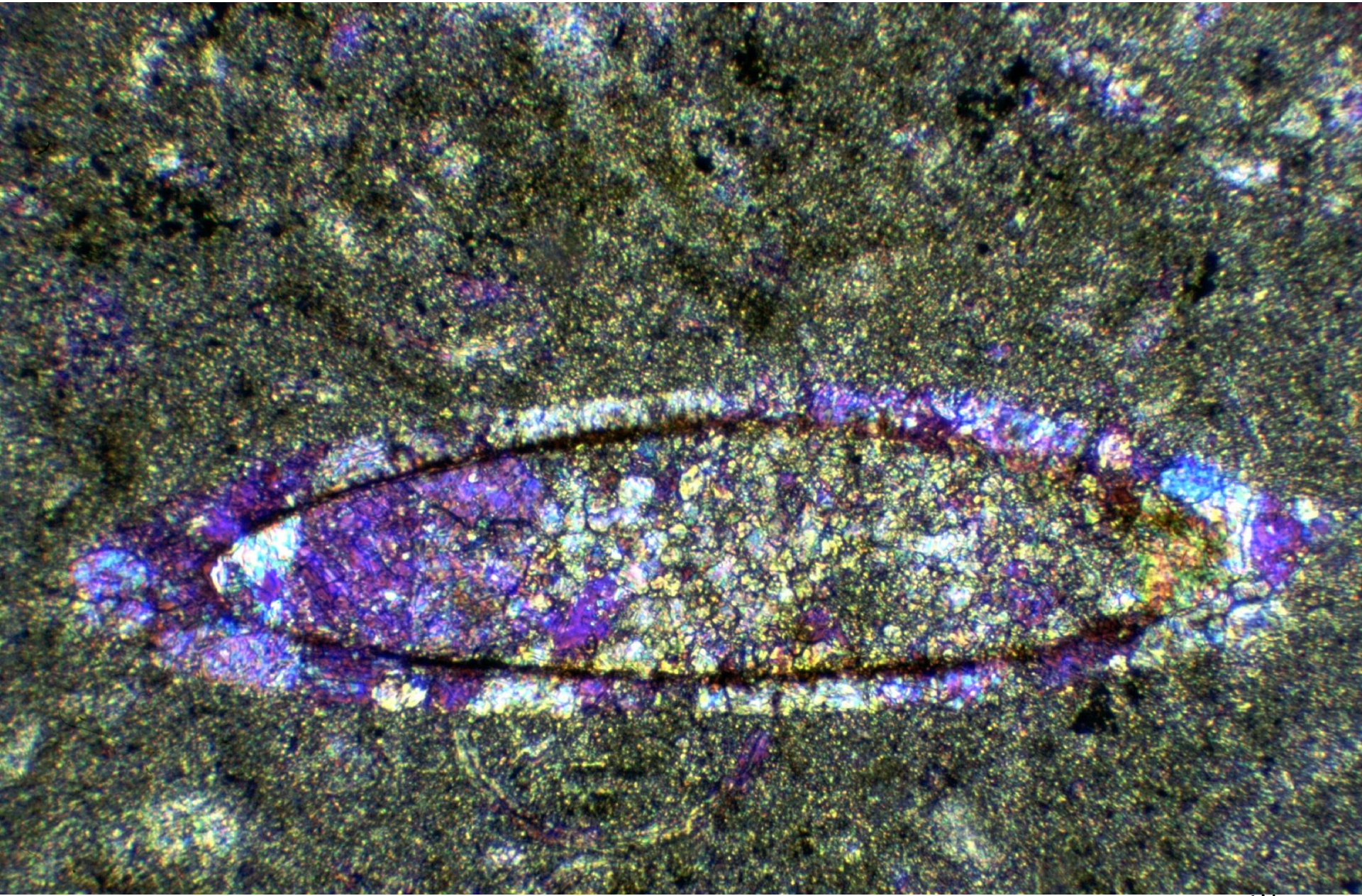
Fig. 4.36 Classification of limestones based on depositional texture. After Dunham (1962) with modifications of Embry & Klovan (1971).

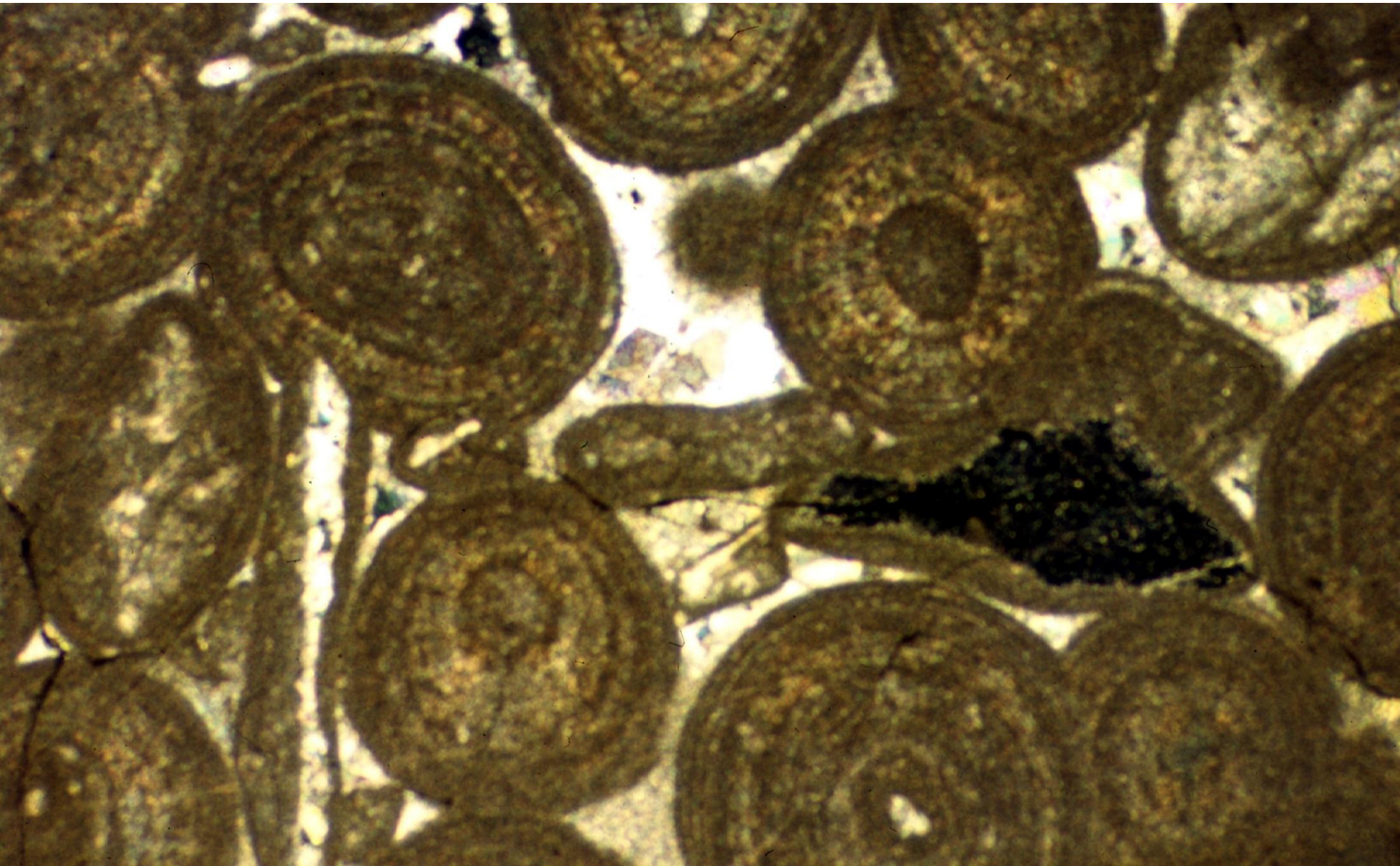


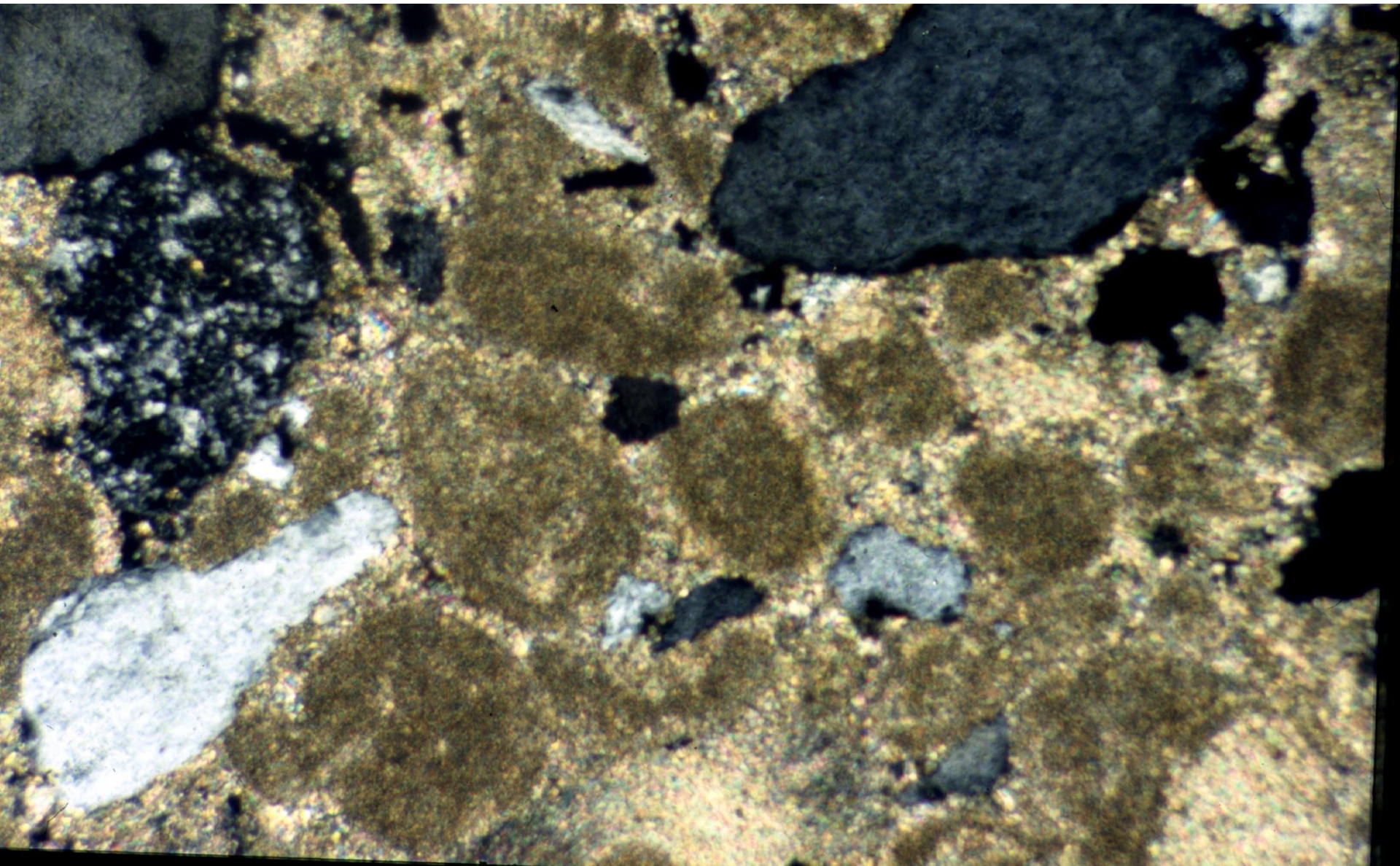


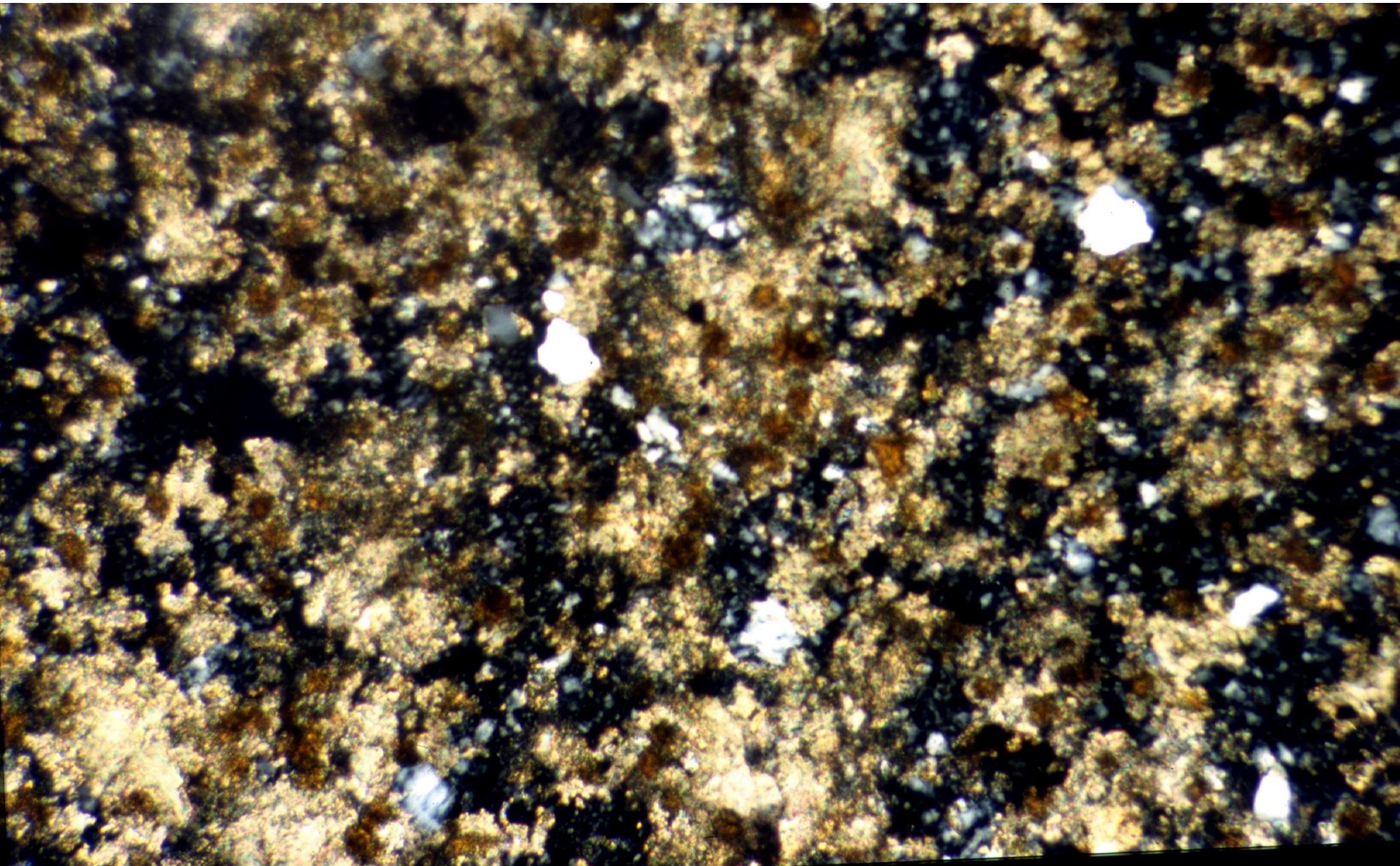


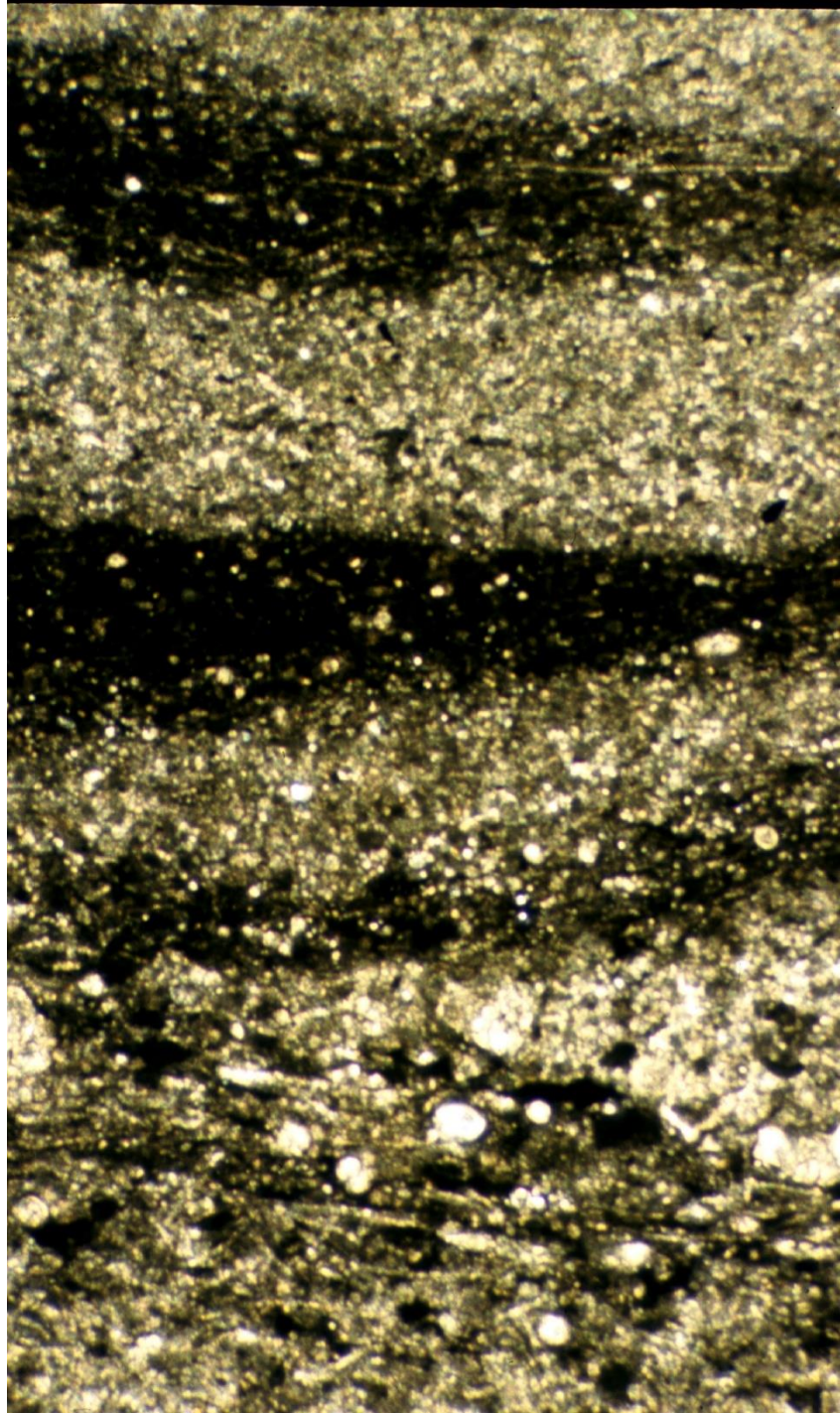


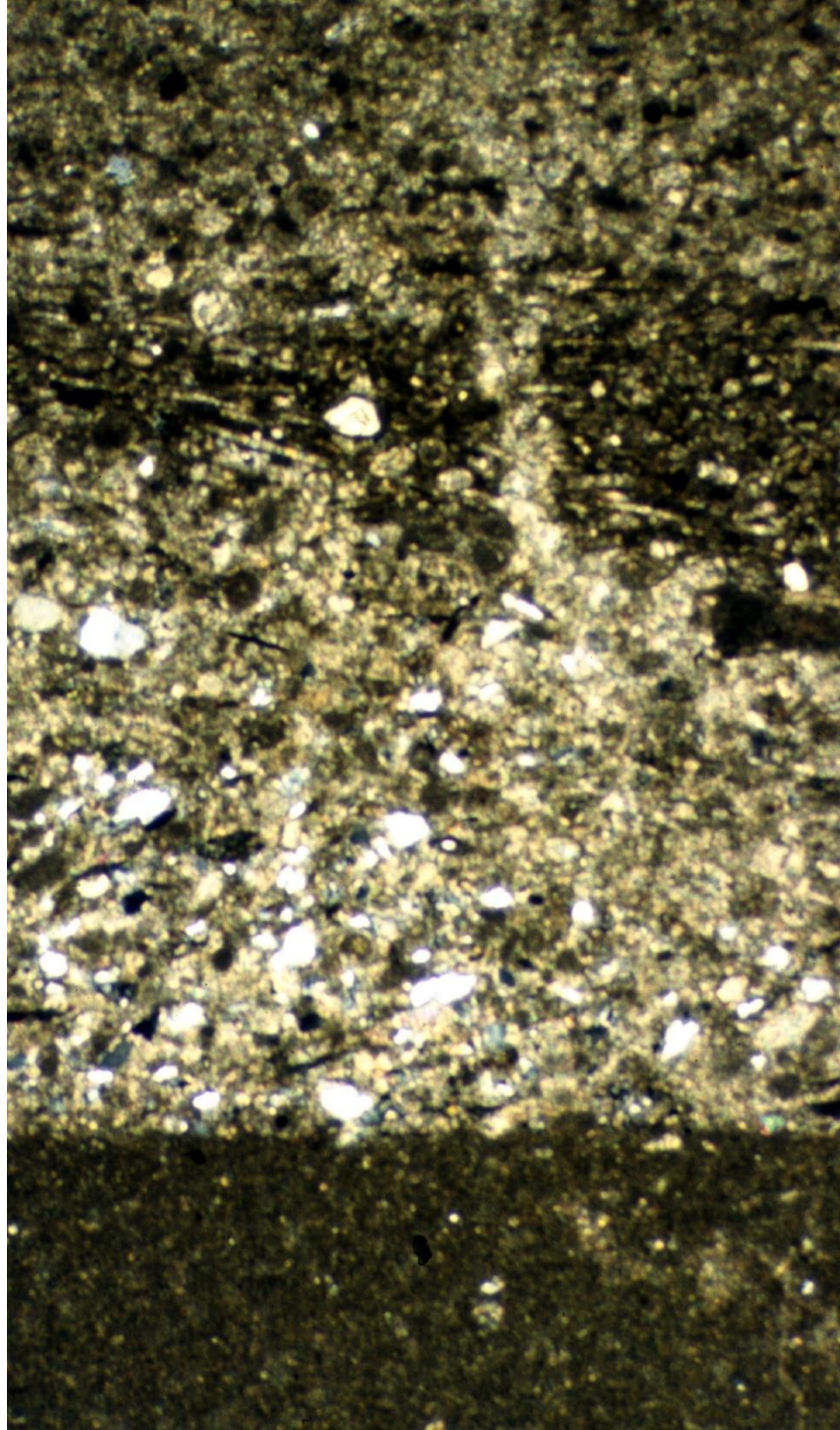












sedimentační prostředí

koncept mikrofacií (Wilson 1975, Flügel 1972, 1982, 2004)

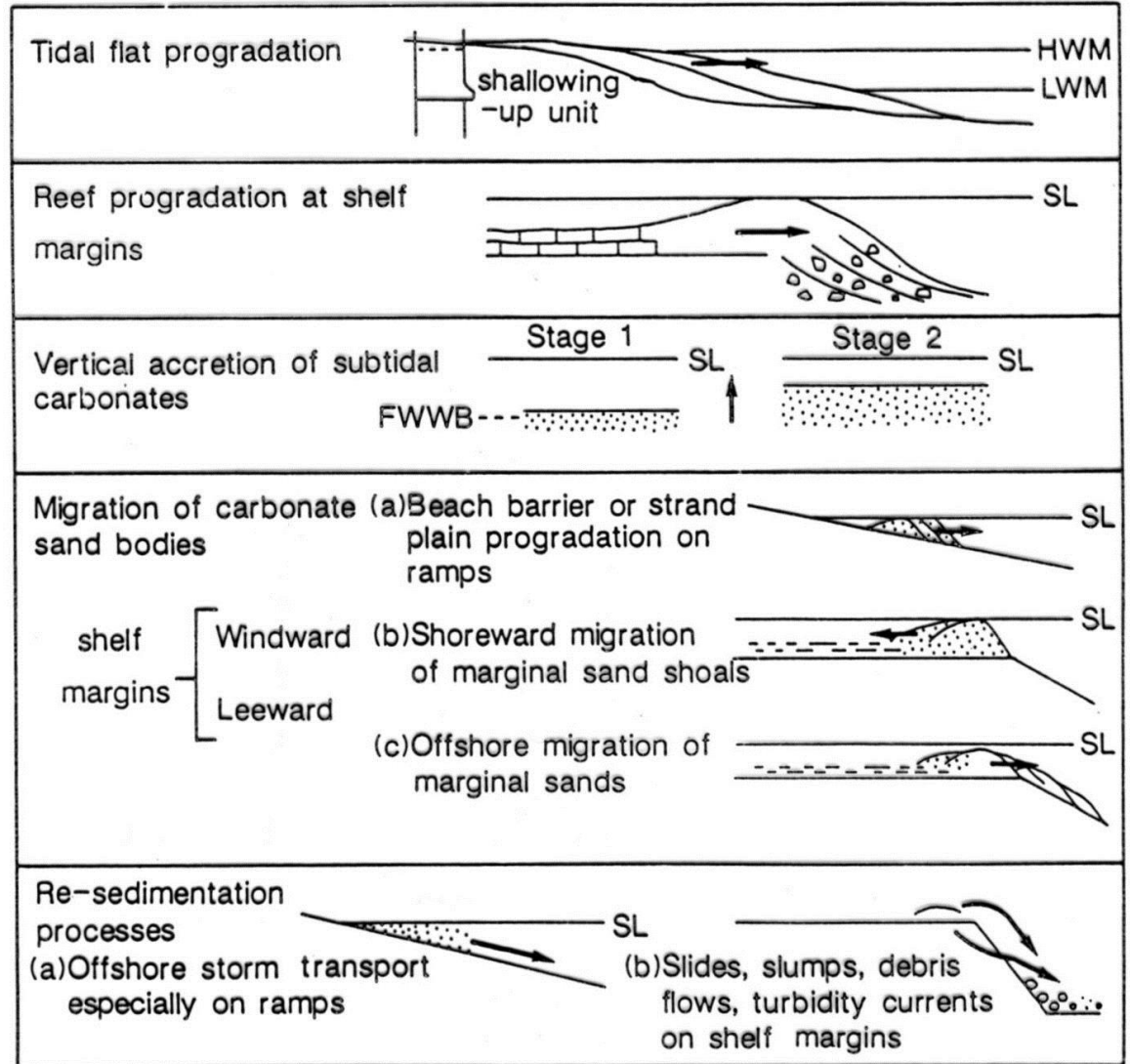


Fig. 2.5 *The principal depositional processes of carbonate sediments. After Tucker (1985a).*

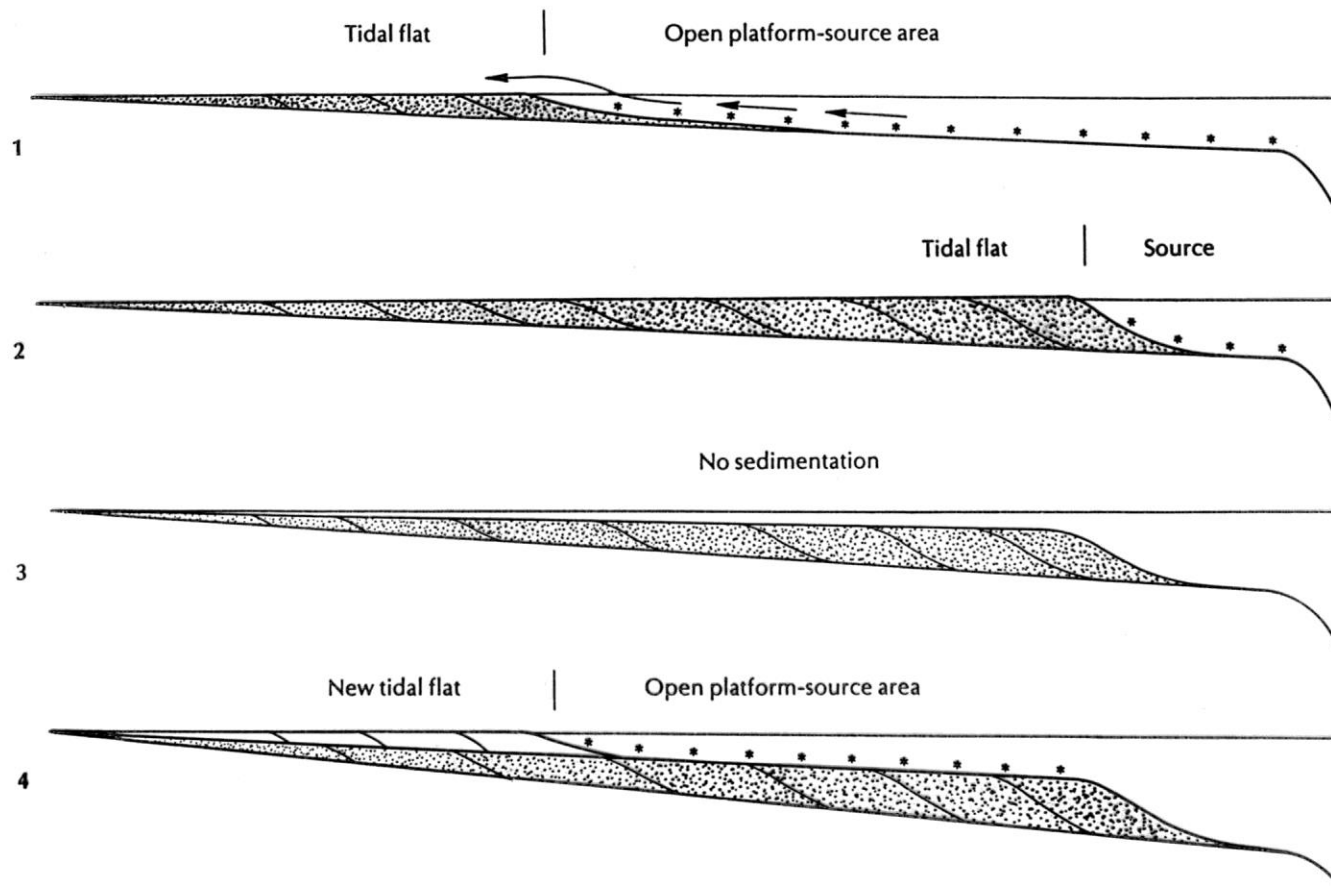


Figure 6.9

A sketch illustrating how two shallowing-upward sequences can be produced by progradation of a tidal flat wedge. These general conditions apply to both eustatic and autocyclic models. The asterisks show areas of carbonate production. From James (1984).

kontinentální - jezerní, pedogeneze, kalkrusty

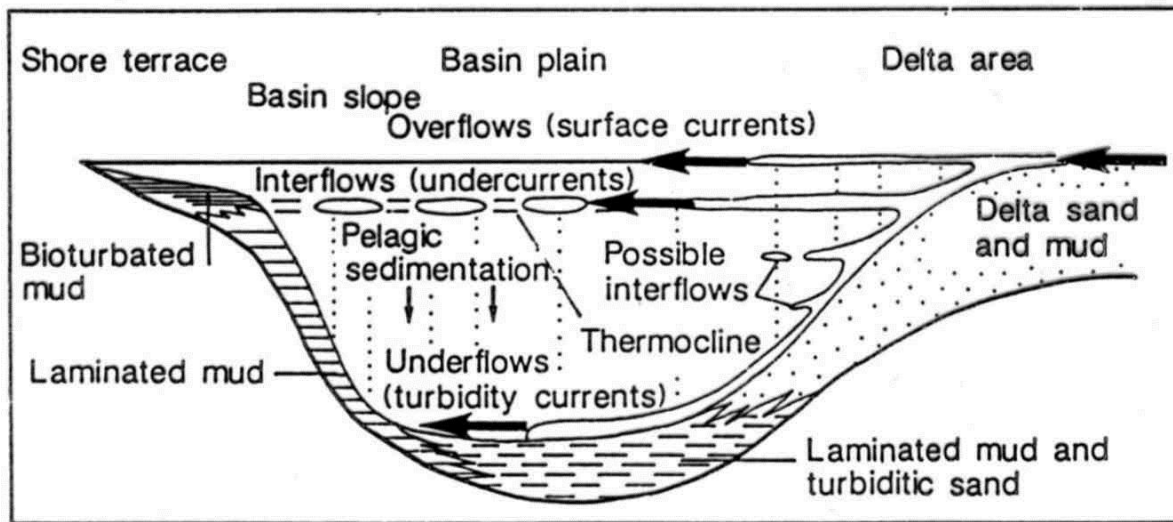


Fig. 4.65 *Sediment dispersal mechanisms and lithofacies for an oligotrophic lake with annual thermal stratification. Based on Sturm & Matter (1978).*

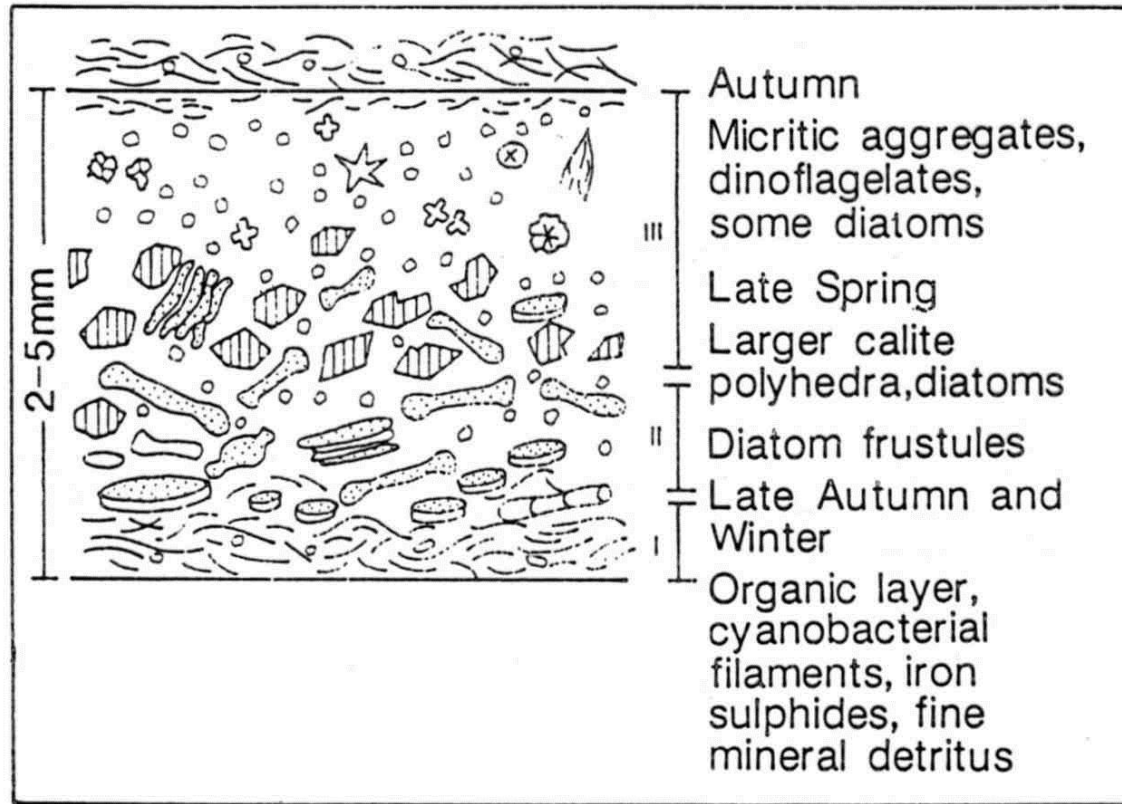


Fig. 4.72 Schematic diagram showing the composition of a triplet from Lake Zurich, Switzerland. Layer I represents settle out from the lake waters. Much of layer II represents diatom blooms. The decreasing crystal size of calcite in layer III reflects changing saturation levels. Modified from Kelts & Hsü (1978); Allen & Collinson (1986).

mořské - karbonátové platformy: hrazený šelf (biohermy, karb. útesy), rampy

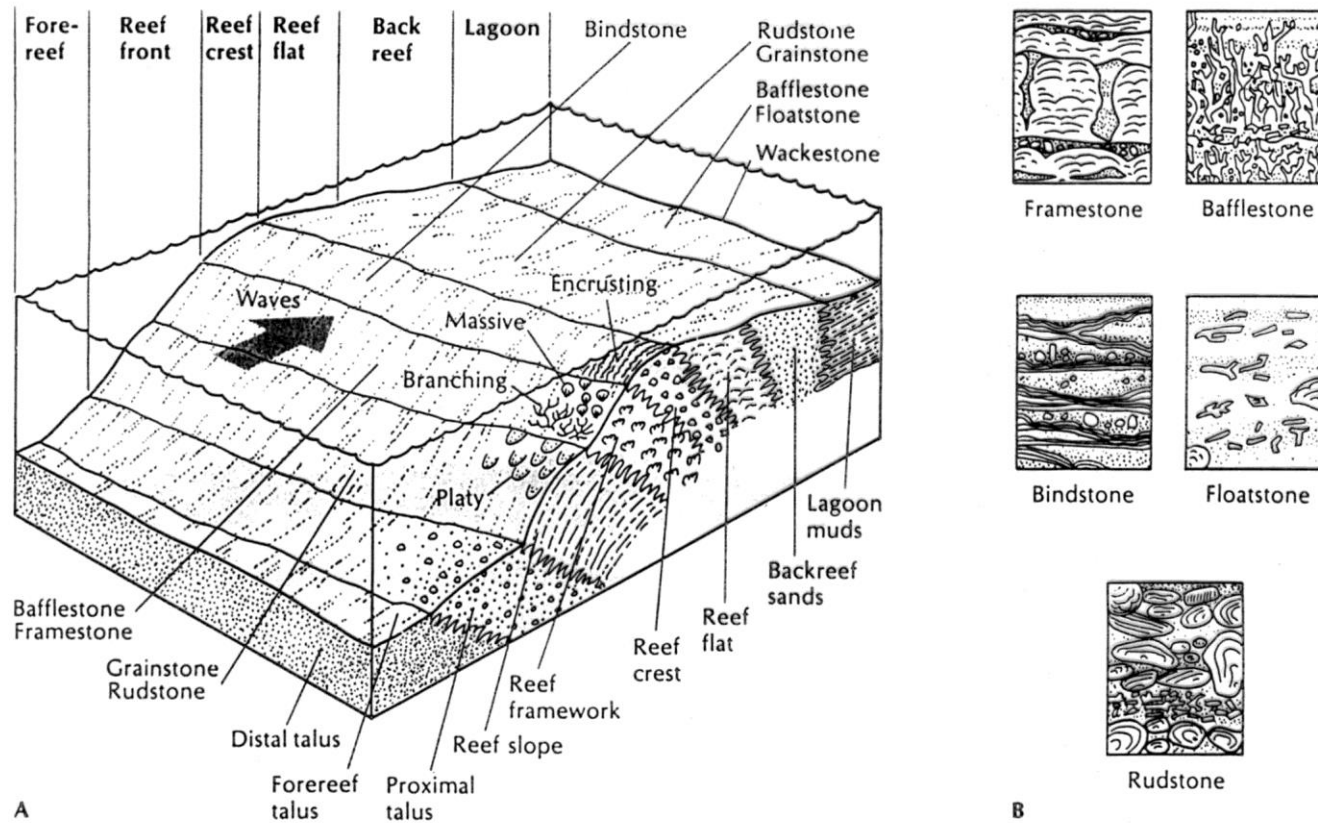
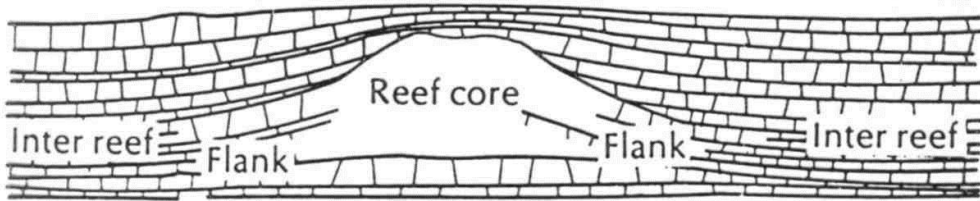
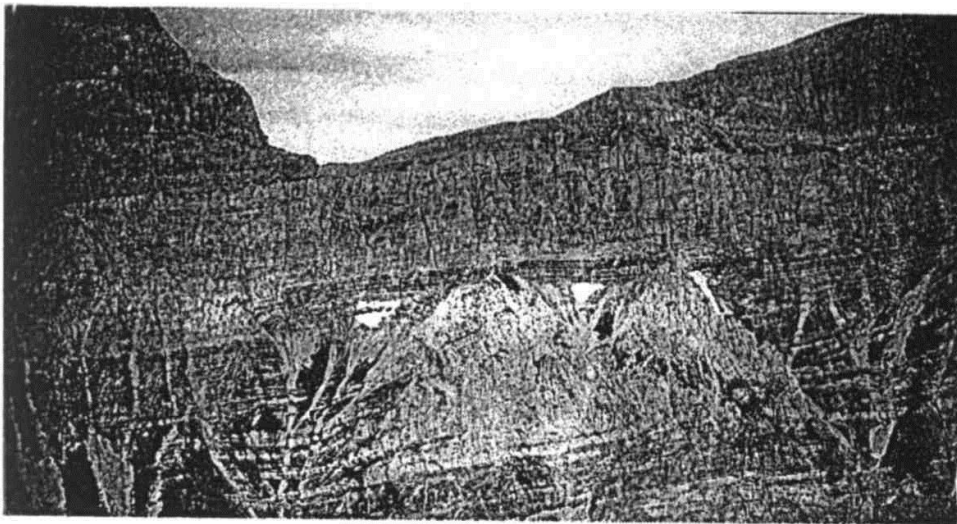


Figure 6.20

(A) Idealized cross section of platform margin reef facies, indicating reef margin zones and the nature of accumulating sediment. After Scoffin (1987). (B) Different types of reef limestone found in these facies, as recognized by Embry and Klovan (1971).



A



B

Figure 6.21

A) A sketch illustrating the three major reef facies in cross section. From Walker (1984). (B) Reef and reef-flank deposits over 100 meters thick, from the Peechee Formation, Upper Devonian, Flathead Range, southern Rocky Mountains, Alberta. R denotes reef core. Photo courtesy B. Pratt.

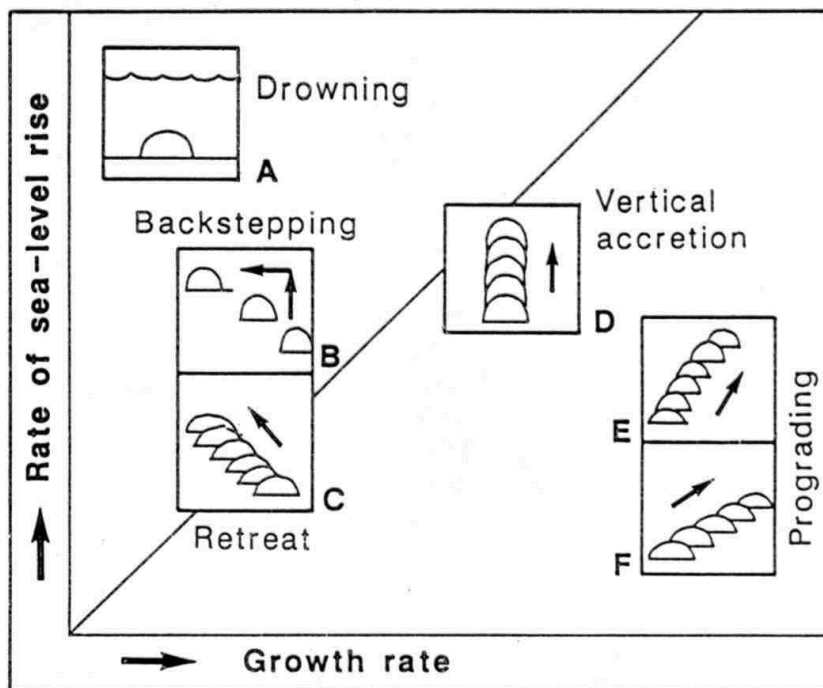


Fig. 4.97 Schematic diagram showing the responses of reefs to sea-level rise. Growth rate refers to the actual accretionary rate of the reef and not to the biological growth rate. In (A), the rate of sea-level rise greatly exceeds the reef growth rate, and the reef is drowned below the depths of biological growth. In (B), the rate of sea-level rise is pulsed allowing recolonization but in progressively shallower waters (backstepped) (Figs 4.98 and 4.99). In (C), the rate of sea-level rise is nearly balanced by accretion and the reef retreats into shallow water. In (D), accretion and sea-level rise are balanced and vertical accretion occurs. In (E) and (F) the rate of sea-level rise is slow enough for the reef to prograde into deeper water (Fig. 4.100). These geometries relate to reefs on shelf or platform edges but isolated reef complexes will show such responses on all sides, although to varying degrees.

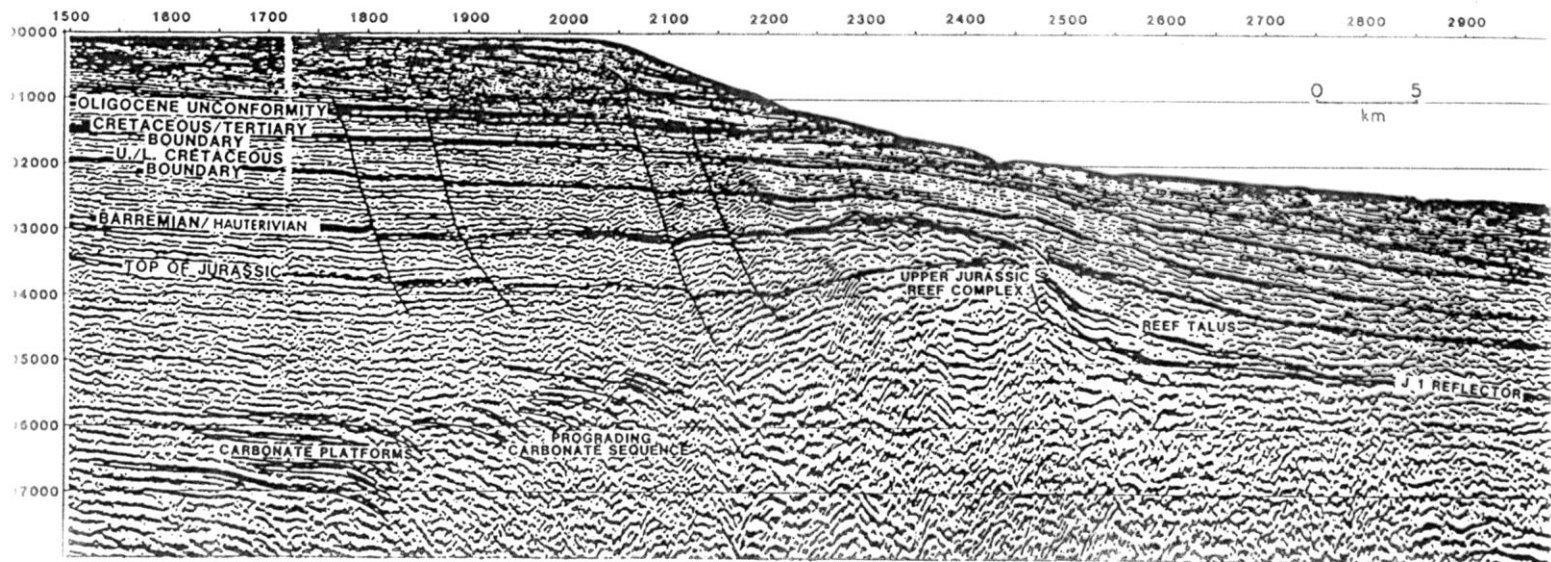


Fig. 6 Seismic reflection profile from the continental margin off northern USA in the region of Baltimore Canyon (offshore from Atlantic City), showing carbonate platforms with prograding ramps and an Upper Jurassic rimmed shelf reef complex with associated reef talus and back-reef, lagoonal deposits. The succeeding Cretaceous–Tertiary sediments are mostly clastics. After Gamboa et al. (1985), courtesy of American Association of Petroleum Geologists.

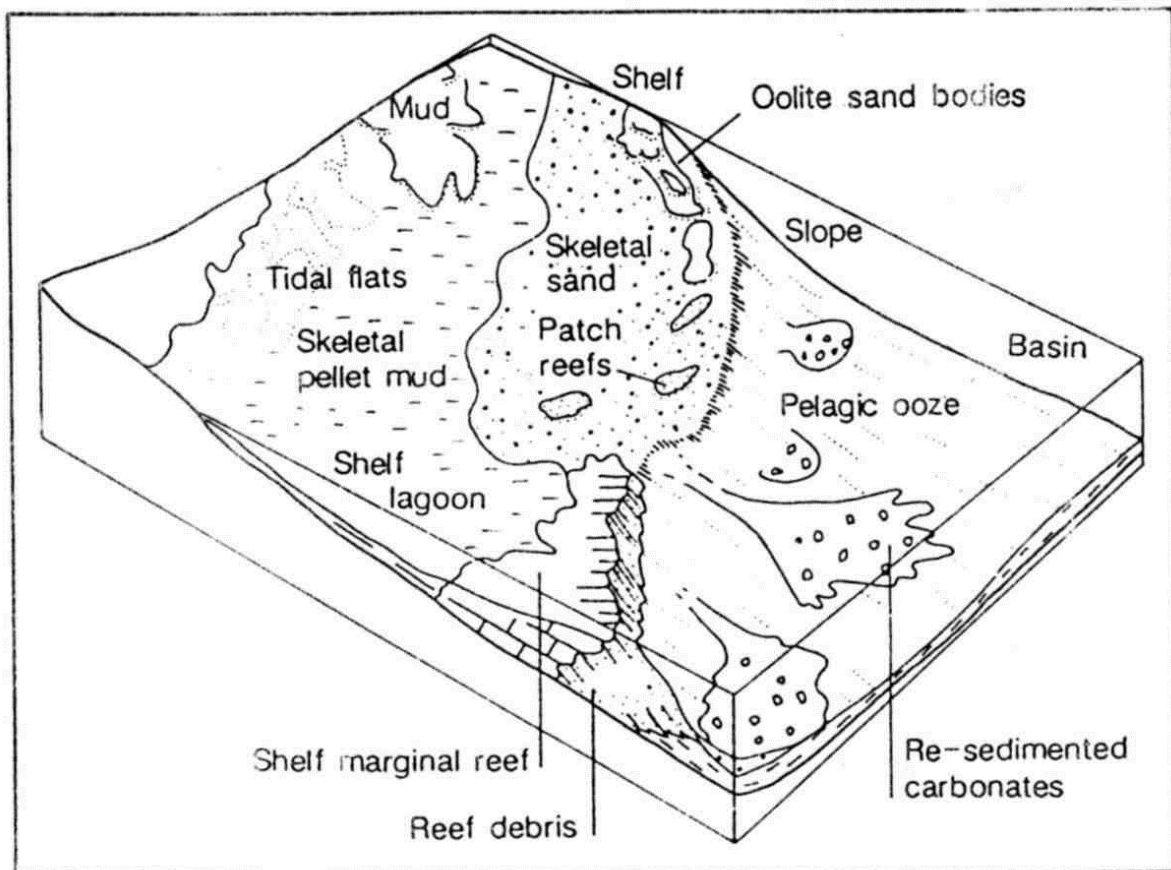


Fig. 2.7 *The carbonate rimmed shelf depositional model. After Tucker (1985a).*

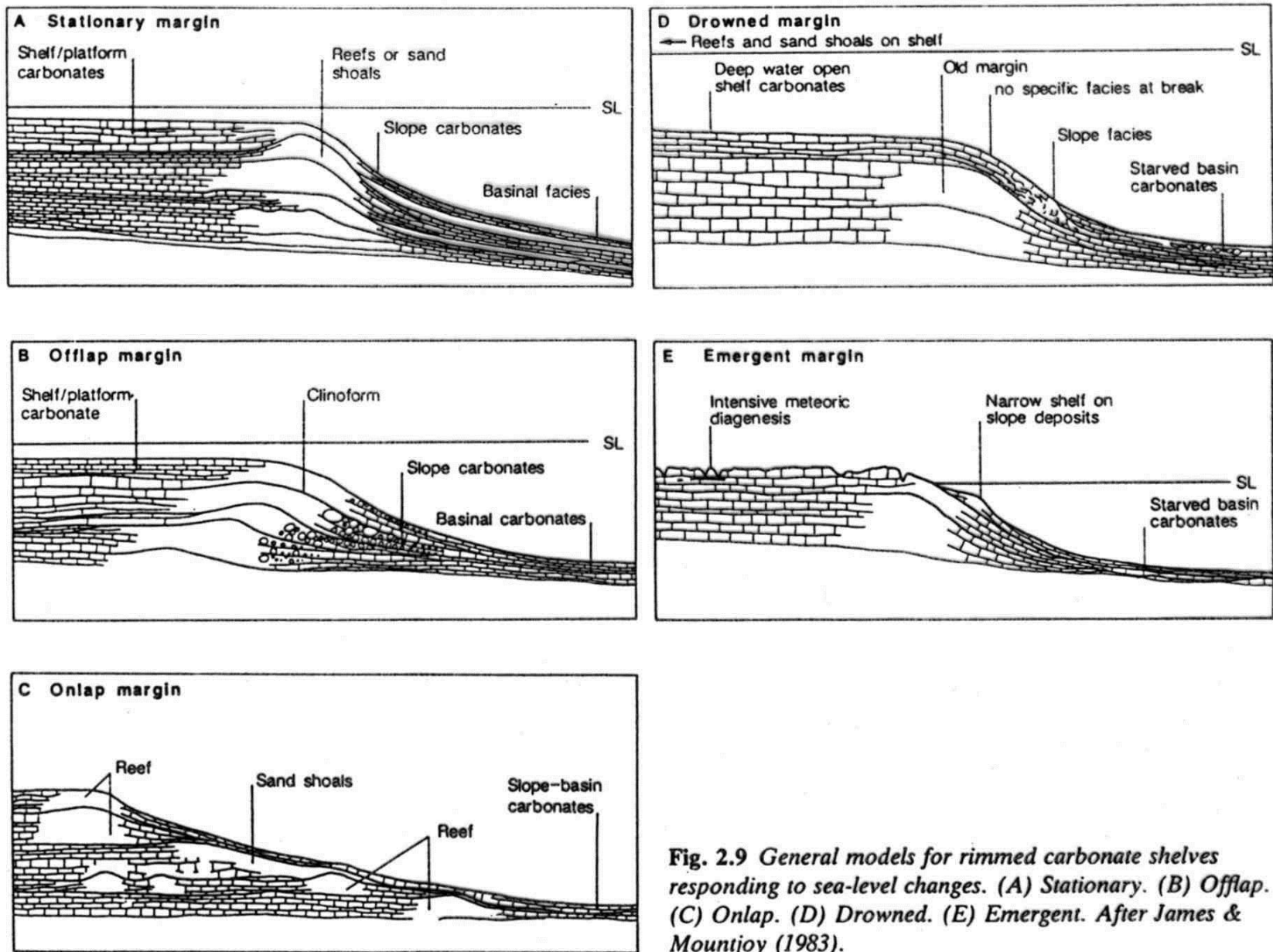


Fig. 2.9 General models for rimmed carbonate shelves responding to sea-level changes. (A) Stationary. (B) Offlap. (C) Onlap. (D) Drowned. (E) Emergent. After James & Mountjoy (1983).

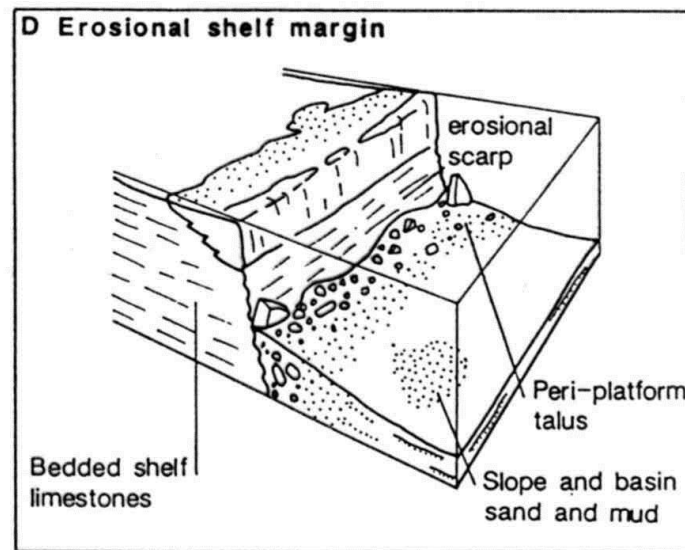
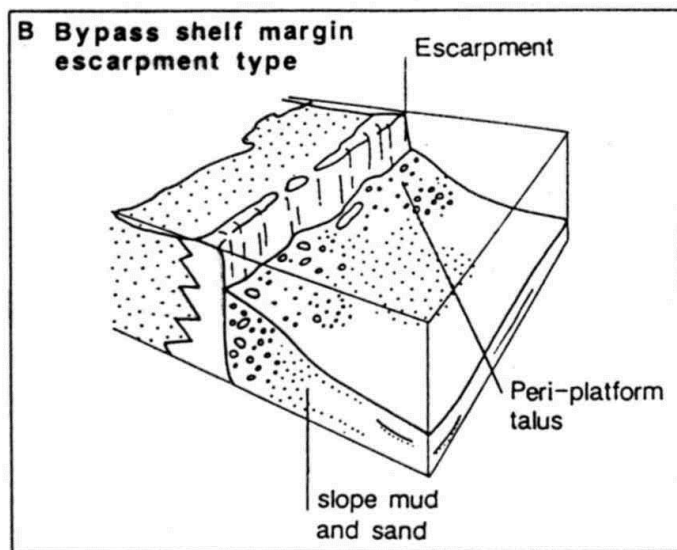
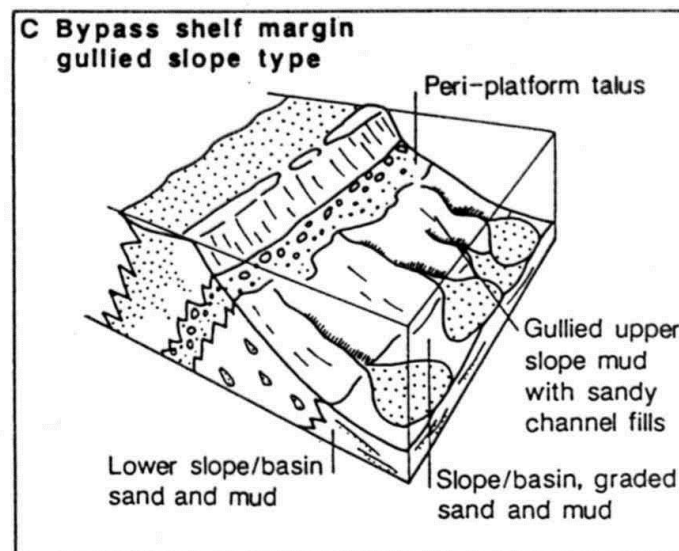
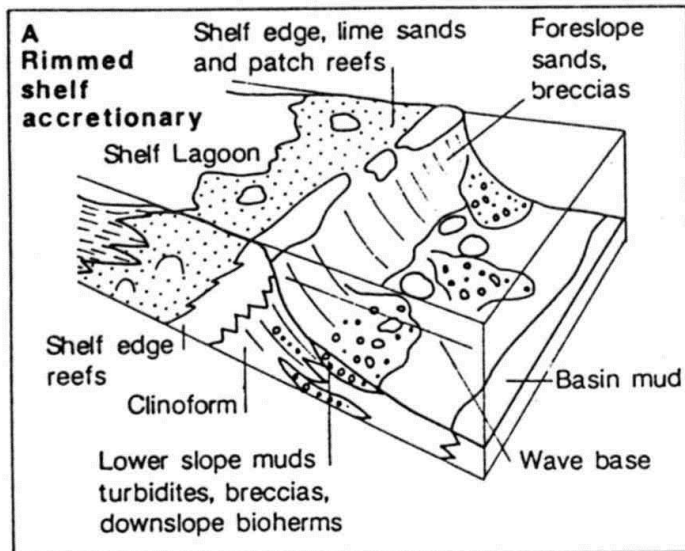


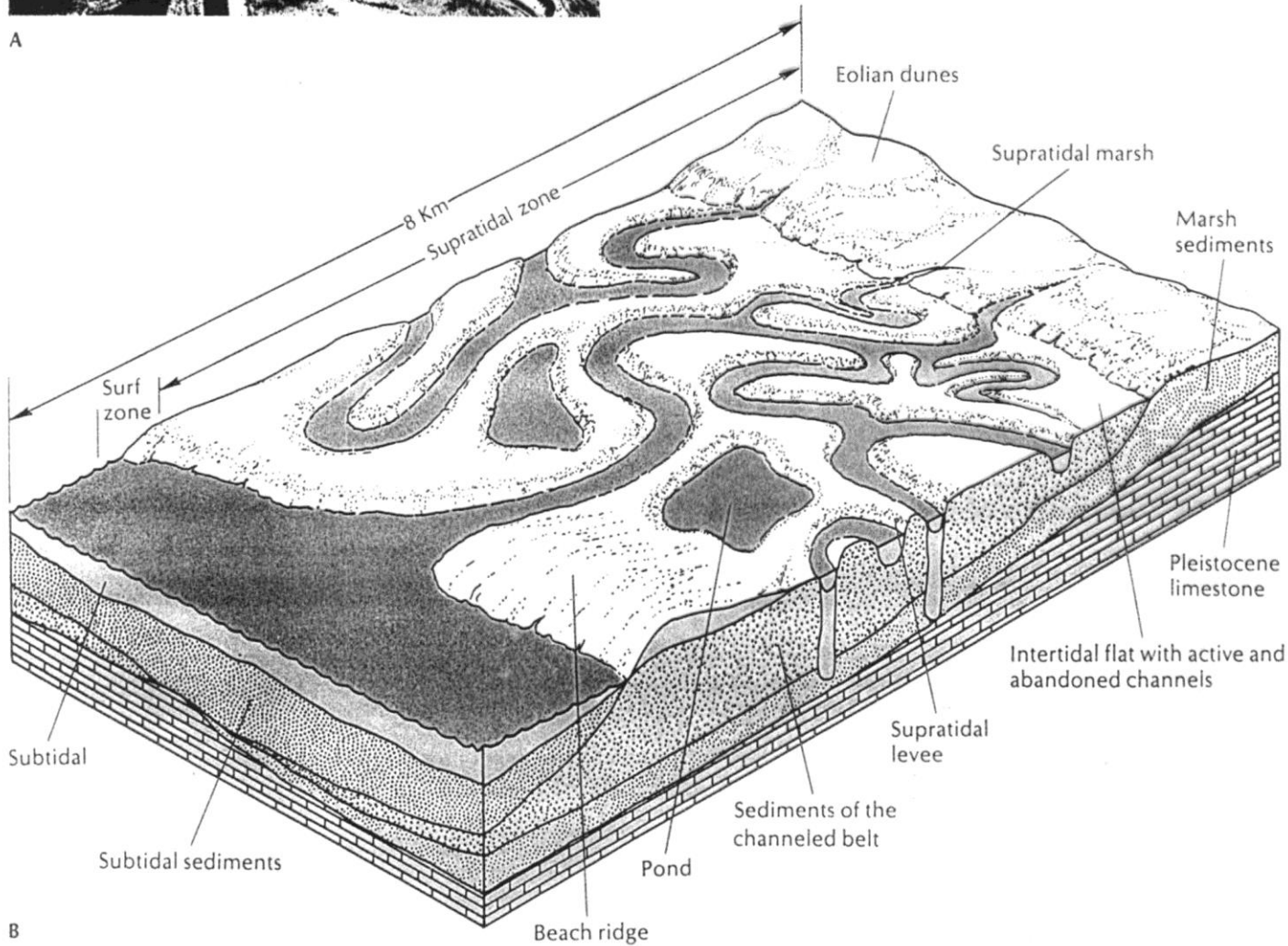
Fig. 2.10 Rimmed carbonate shelf types. (A) Accretionary type. (B) Bypass, escarpment type. (C) Bypass, gullied-slope type. (D) Erosional rimmed shelf margin. After Road (1982).



Figure 6.2

(A) The Three Creeks area along the west coast of Andros Island, Bahamas; tidal channels cut an intertidal marsh composed largely of algae, with some ponds in the intertidal areas. (B) Diagram showing major features of the peritidal environment. From Stanley (1989).

intertidál - supratidál



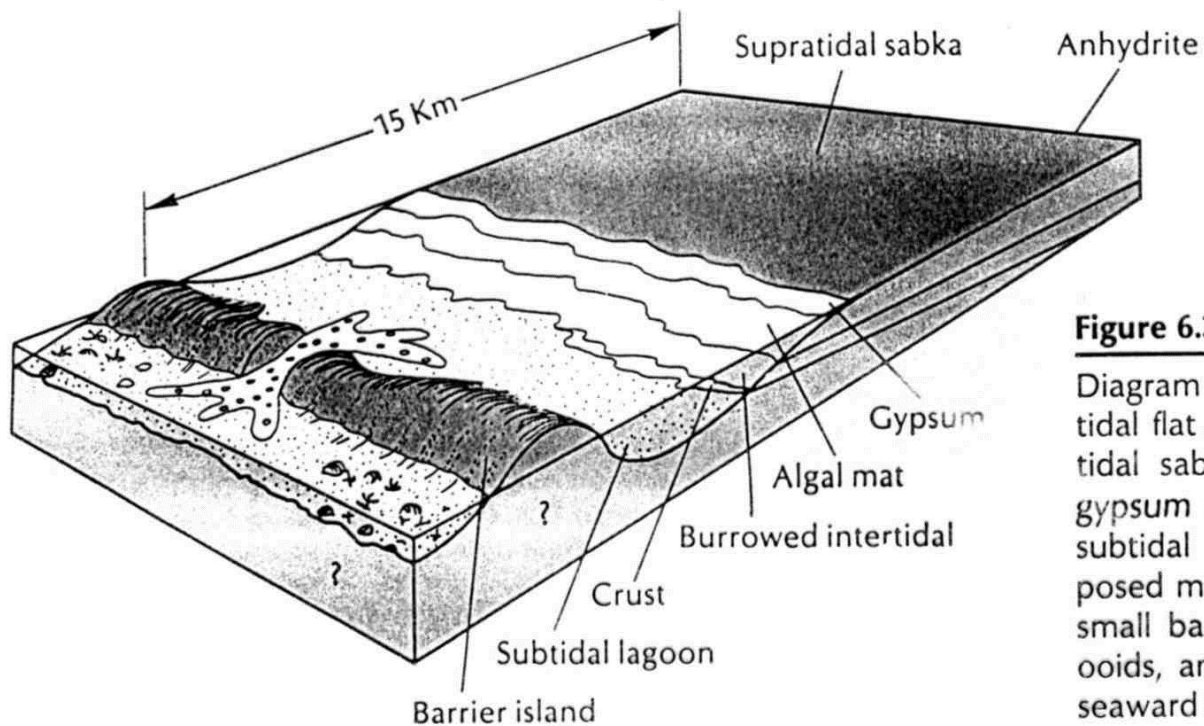


Figure 6.3

Diagram showing the major facies of the regressive tidal flat on the Persian Gulf Trucial Coast. Supratidal sabkha is composed of algal mats with a gypsum crust, which have grown over burrowed subtidal lagoonal sediments. Tidal deltas, composed mainly of ooids, form around inlets cut into small barrier islands composed of mollusc shells, ooids, and coral fragments. Coral reefs can grow seaward of the island, away from the tidal inlets.

lagunární karbonáty

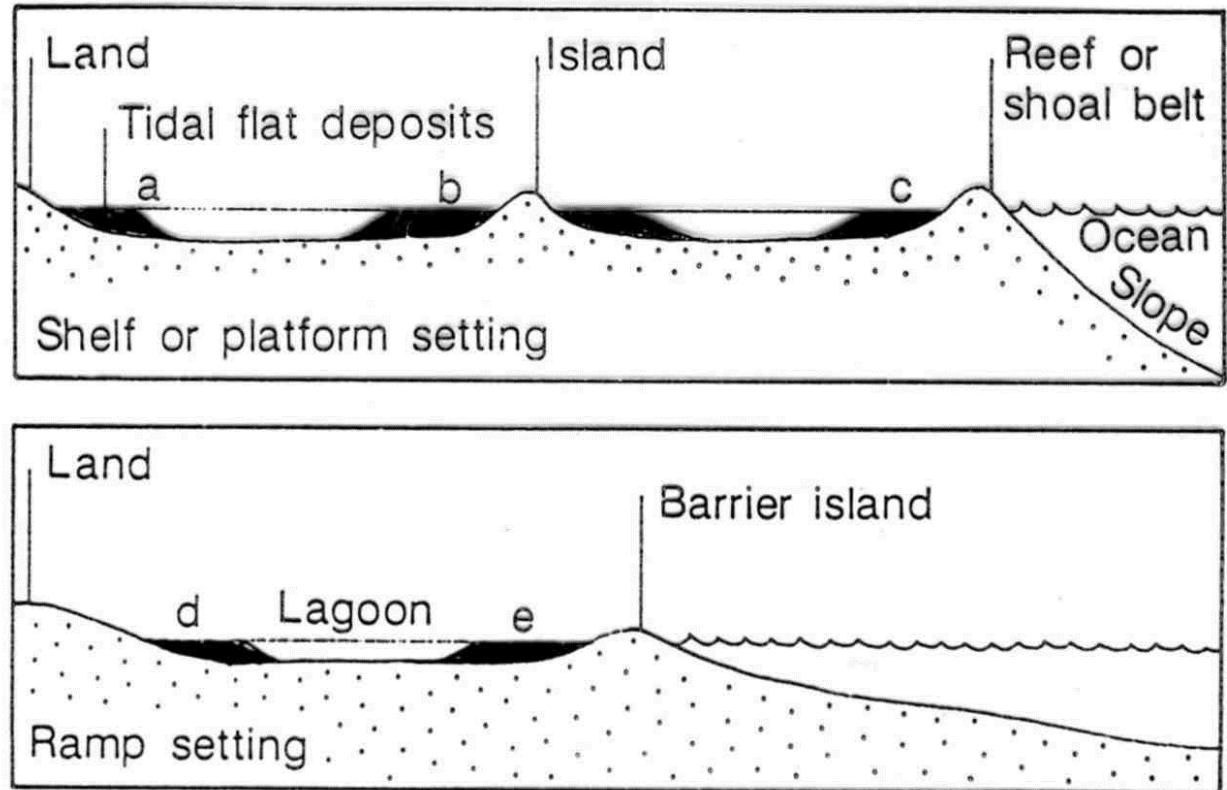


Fig. 4.39 Sites of tidal flat deposition on shelves/platforms and ramps. Examples: (a) Florida Bay; (b) shelf islands of Belize (Ebanks, 1975) and Lower Ordovician of Newfoundland (Pratt & James, 1986); (c) Andros Island, Bahamas (Chapter 3); (d) and (e) Trucial Coast of Arabian Gulf.

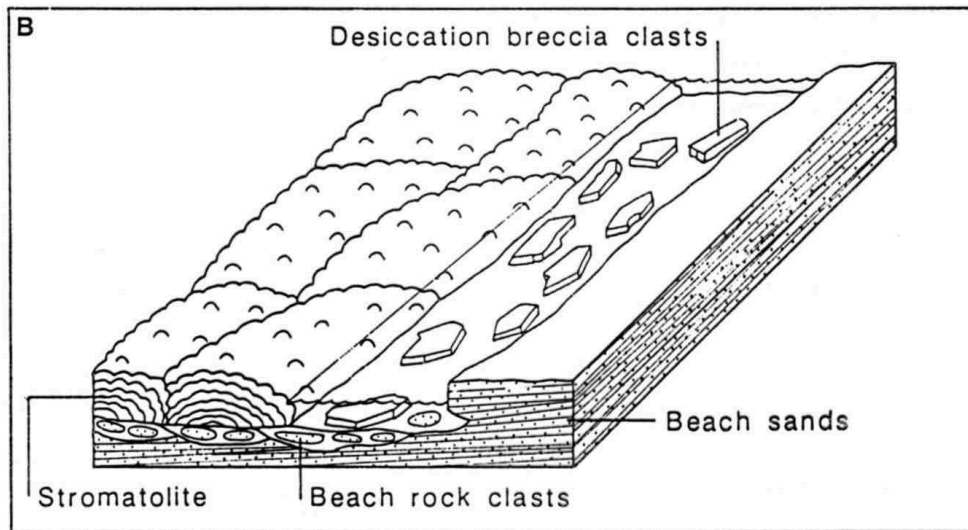
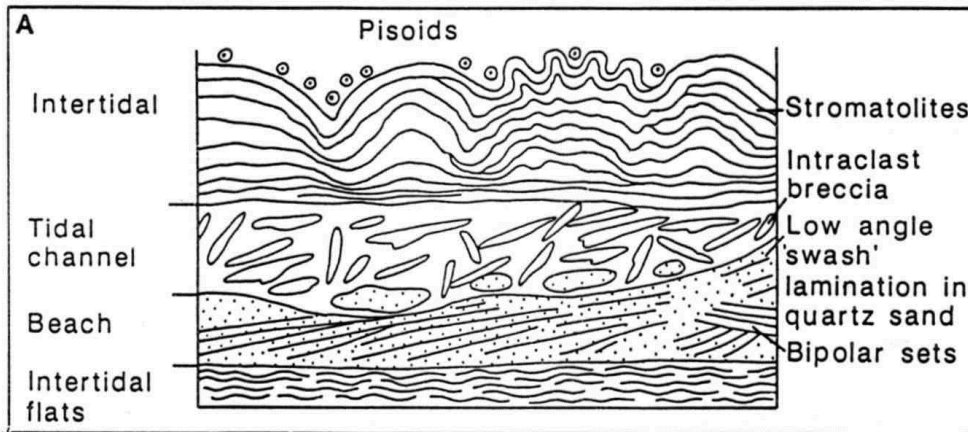


Fig. 4.42 Tidal channels from Late Precambrian Khufai Formation, central Oman. (A) Schematic of tidal channel sequence, which ranges from 0.3 to 1.0 m in thickness. Cross-laminated beach deposits (siliciclastic sands) are erosively truncated by channel forms filled by desiccation breccias. Stromatolites cap these channel fills. (B) Reconstruction of tidal channel. After Wright et al. (1989).

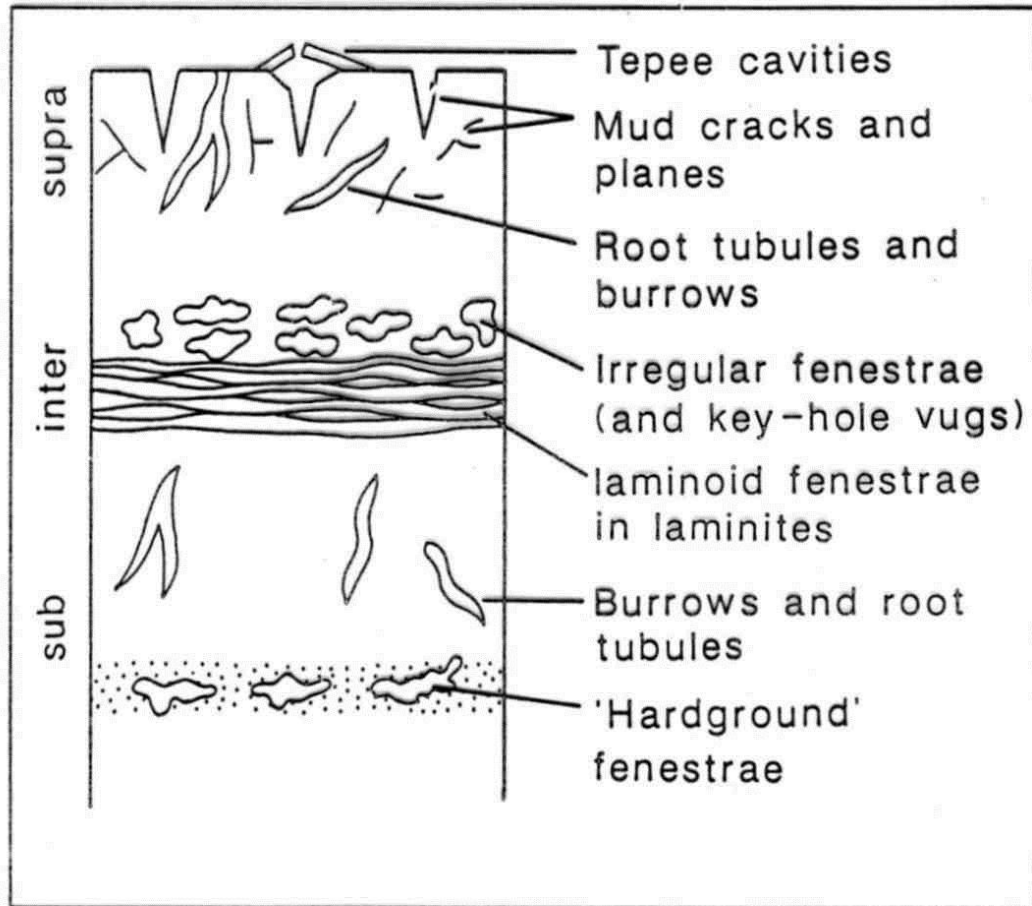


Fig. 4.47 *Open-space structures in peritidal deposits (see text). Planes are fractures, and is a term used by soil scientists for open cracks.*

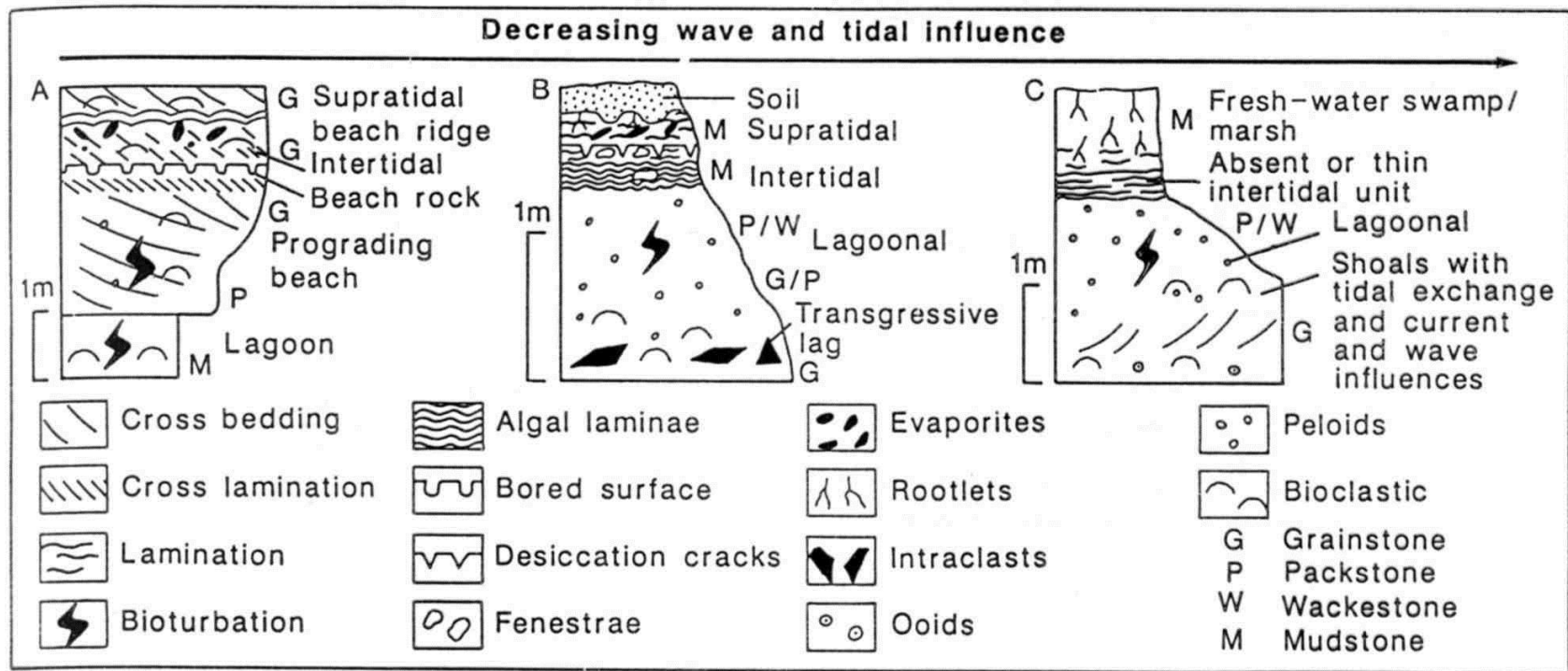


Fig. 4.55 Spectrum of peritidal shoaling units reflecting differing degrees of wave and tidal influence. (A) High-energy type based on Khor Duwahine, extreme western part of Abu Dhabi; although this area is protected from the Shamal winds it still lacks protection by a barrier system and is wave influenced. Microbial mats only occur on the upper part of the intertidal zone and are associated with evaporites (gypsum). These sand flats are prograding seawards with an accretion slope showing seawards-inclined bedding. Based on data in Purser & Evans (1973). (B) Protected, lower-energy sequence. The initial coarse transgressive lag horizon is followed by a shoaling phase showing well-defined intertidal facies. Based on Lower Carboniferous peritidal deposits from south Wales (Wright, 1986a); similar sequences are shown by James (1984a). (C) Highly restricted sequence; shoaling from a grainstone facies, with wave and tidal influences, into lagoonal and finally a freshwater facies (supratidal-terrestrial). Intertidal deposits are thin or absent. Based on data in Palmer (1979) for the Middle Jurassic White Limestone Formation (Fig. 4.53). This sequence is broadly comparable to the transition across the present-day Florida Shelf lagoon. Wave action and tidal exchange are greatly reduced over the shelf which results in nearshore areas being effectively tideless. In contrast to (A) and (B) this sequence has formed under a more humid climate and lacks evaporites. Diagram modified from Wright (1984).

intertidál – subtidál
písčítá tělesa
karb. šelf

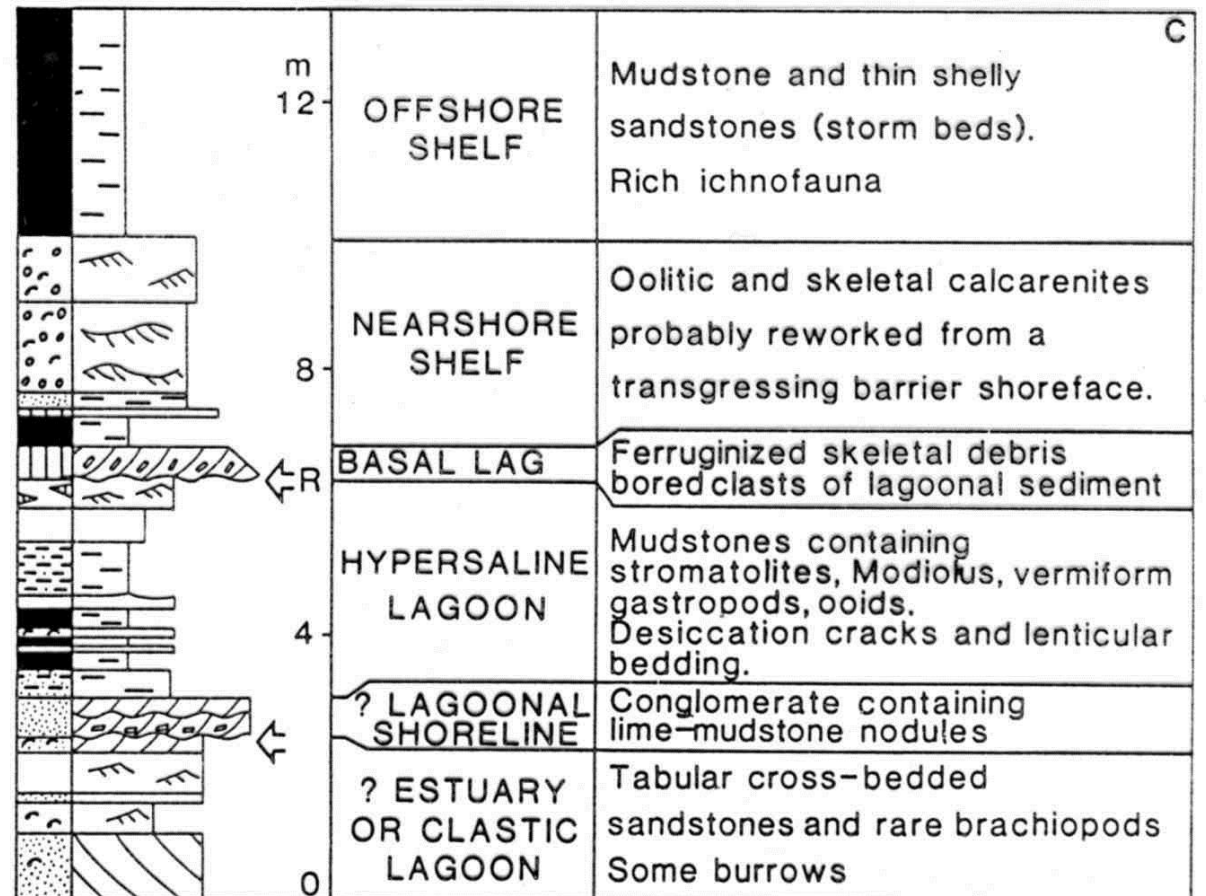
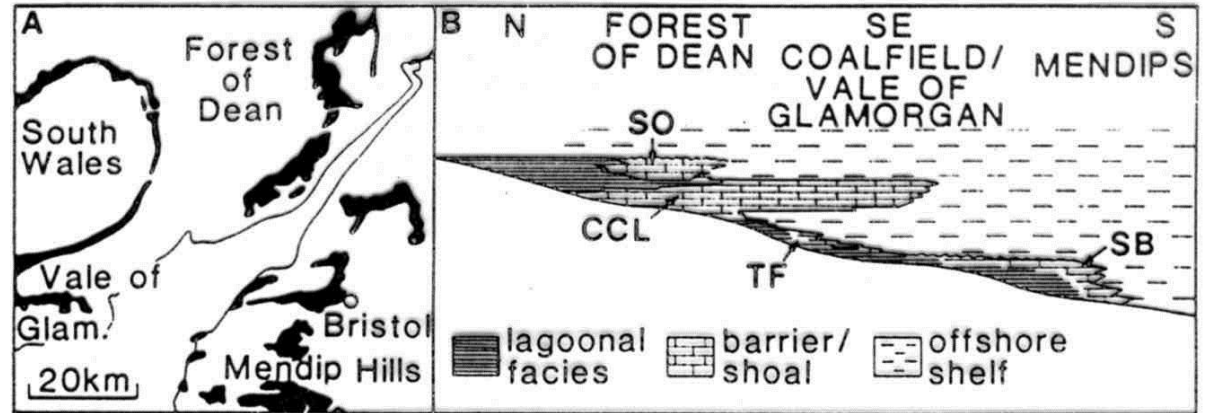
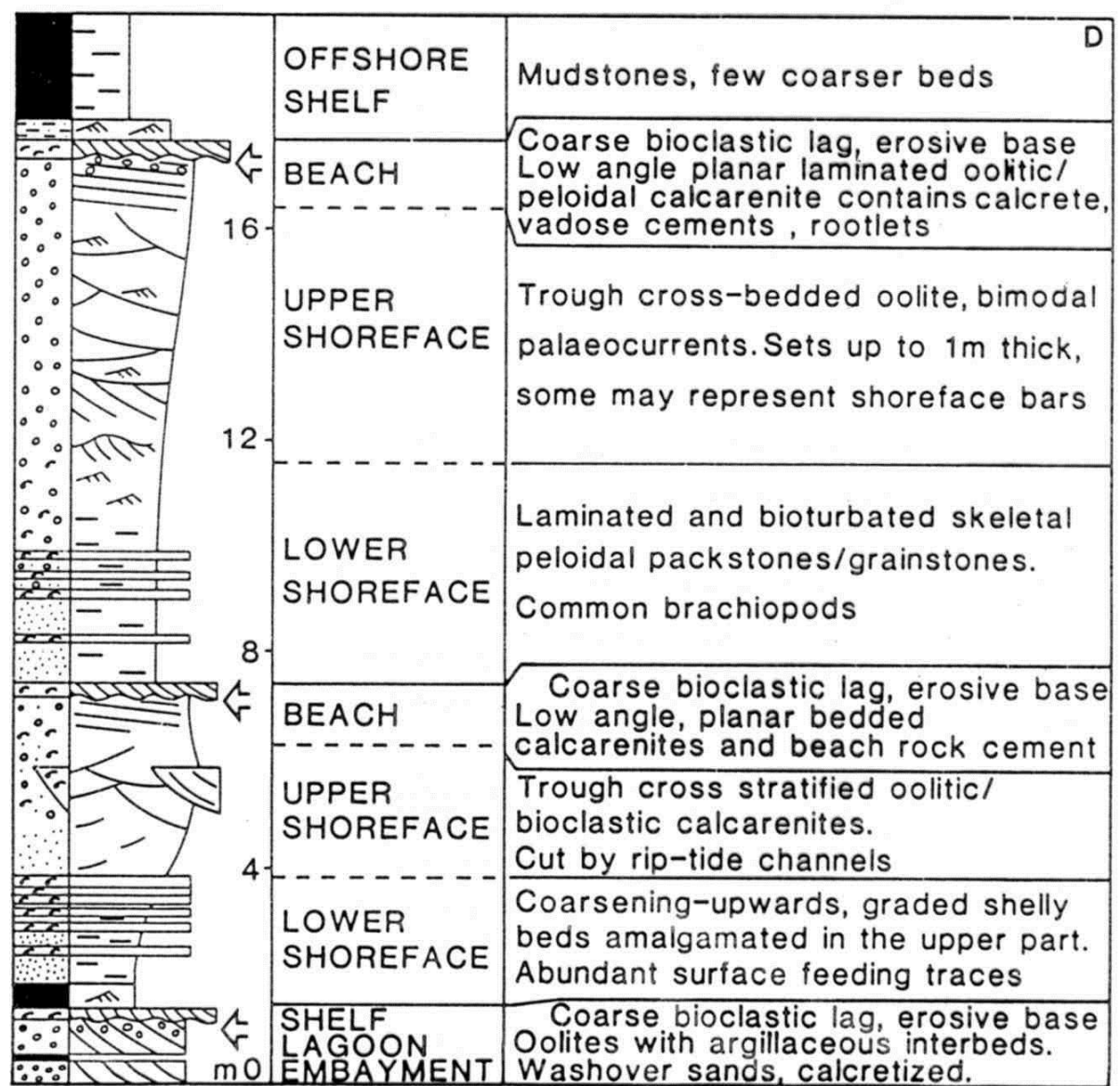
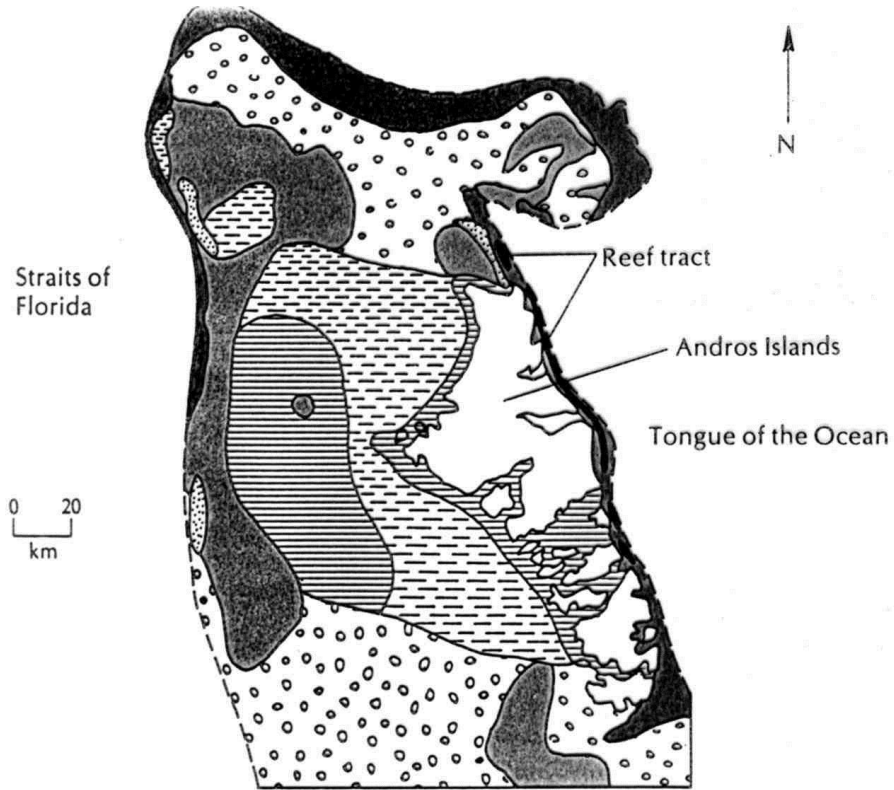


Fig. 4.23 Beach-barrier–lagoon complexes in the Lower Carboniferous (Tournasian) of southwest UK. (A) Location and outcrop map. (B) Stratigraphic cross-section showing three barrier developments: (1) Shirehampton Beds–Tongwynlais Formation (SB and TF), a transgressive barrier, (2) Castell Coch Limestone (CCL), a regressive barrier, and (3) the Stowe Oolite (SO), of two regressive shoreface to beach sequences with lagoonal sediments behind. (C) Simplified log of lower Tongwynlais Formation. Arrows indicate a ravinement (R) and strong erosion surface. (D) Simplified log of Stowe Oolite showing two stacked shoaling sequences from shoreline progradation. After Burchette (1987).

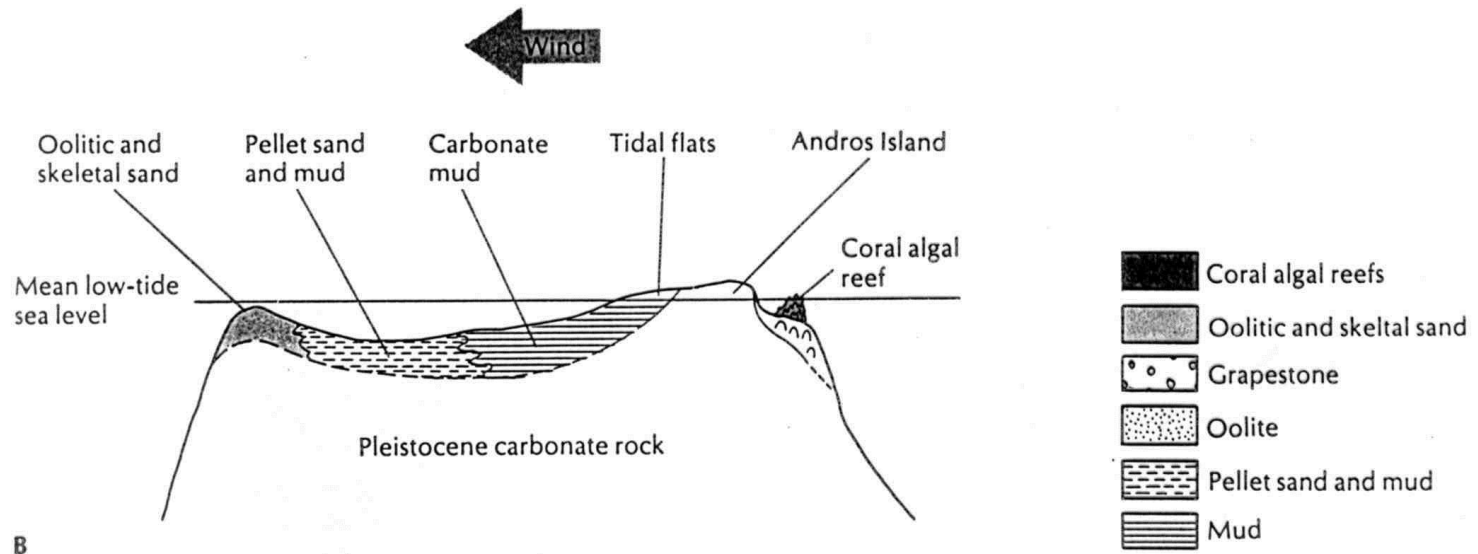




A

Figure 6.10

(A) Generalized map of the carbonate facies of the Bahama Banks near Andros Island. From Sellwood (1978). (B) Cross section of the Bahamas Banks, showing principal facies. From Blatt et al. (1980).



B

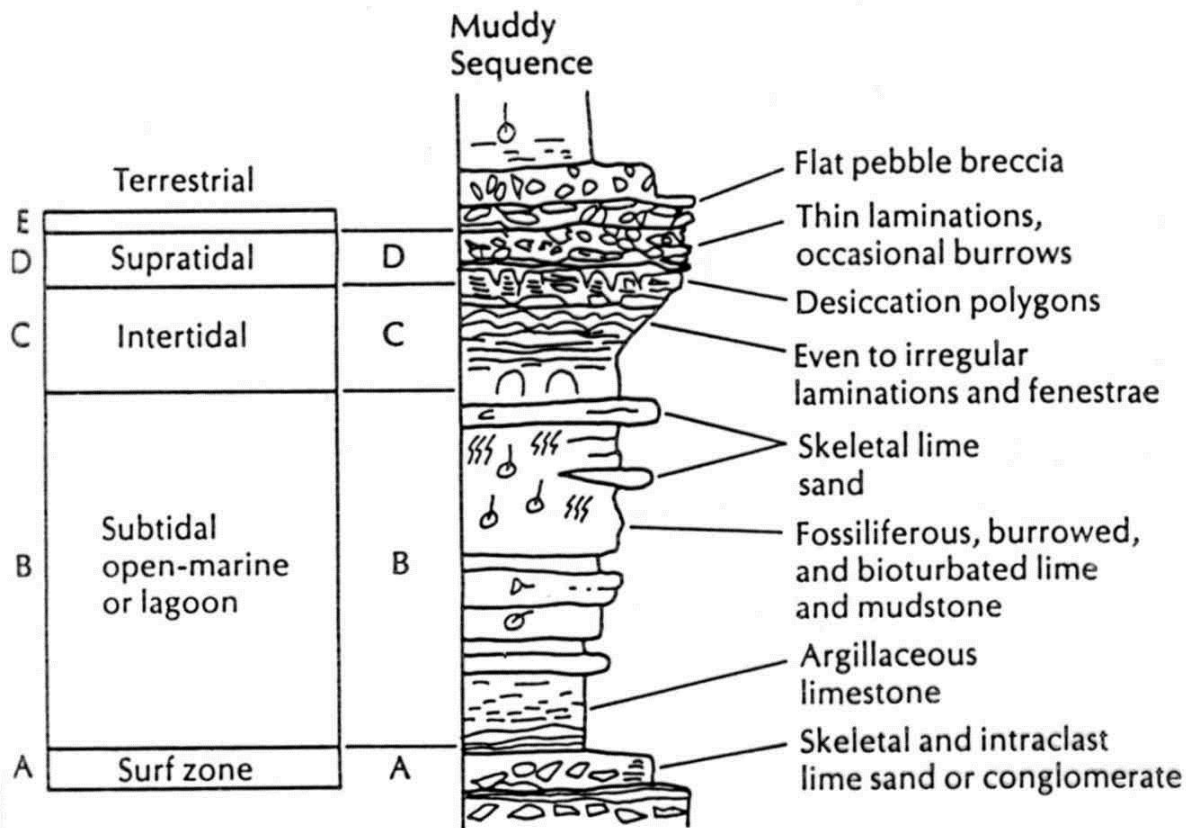


Figure 6.13

Hypothetical shallowing-upward sequence on a low-energy carbonate shelf. From James (1984).

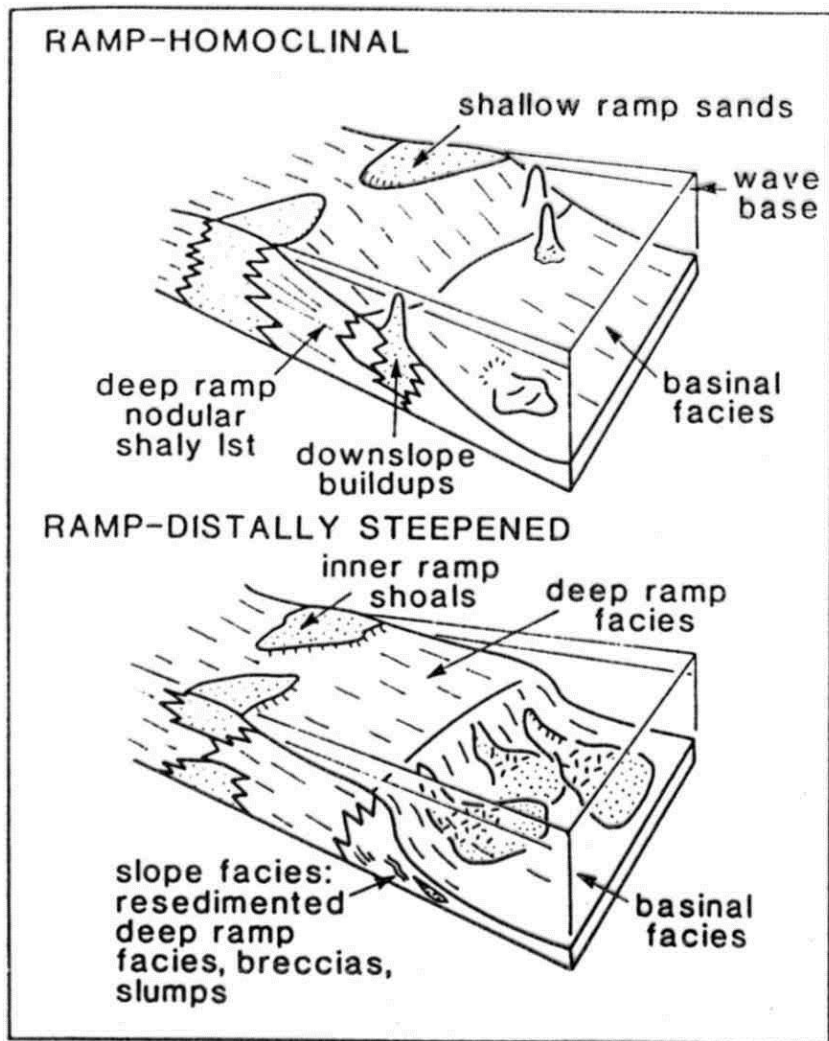


Fig. 2.18 Two types of ramp: homoclinal and distally steepened. After Read (1982).

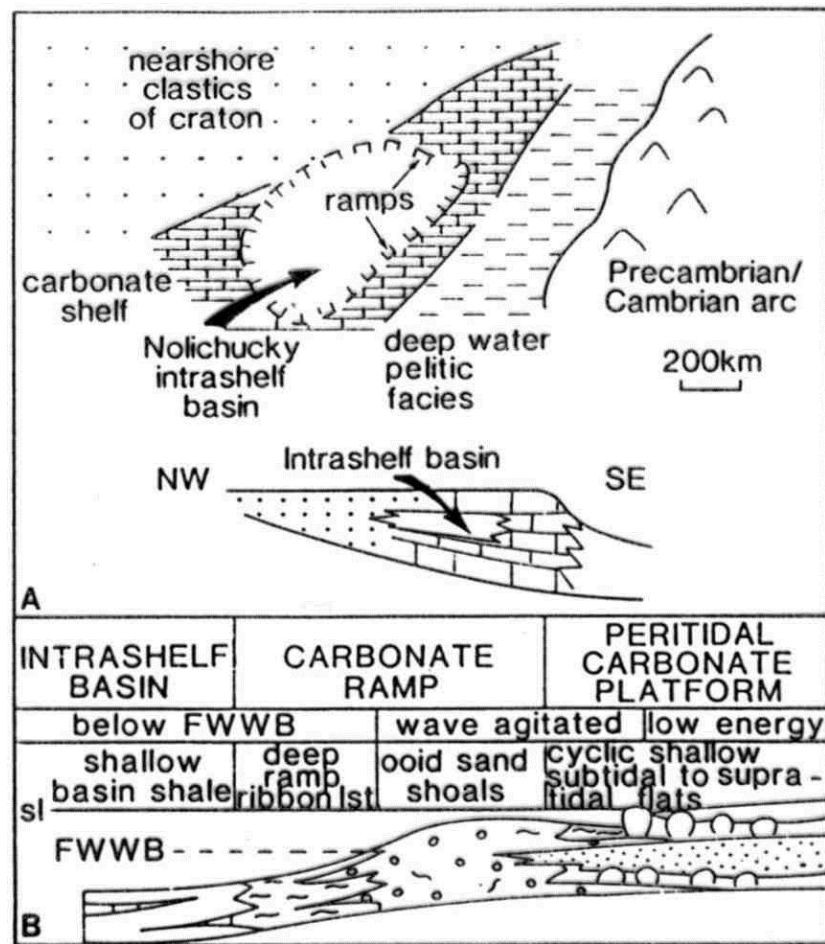


Fig. 2.19 Upper Cambrian carbonate shelf, ramps, intrashelf basin and ramp facies model of the southern Appalachians, USA. After Markello & Read (1981).

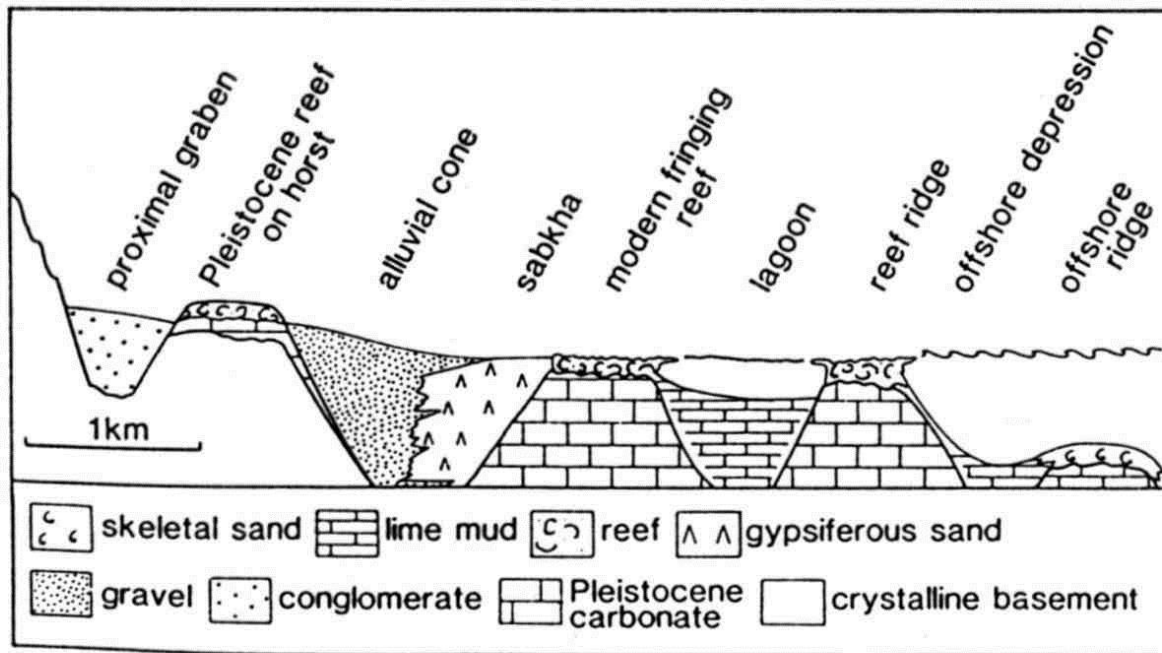


Fig. 2.24 Schematic cross-section of the western Red Sea shoreline area showing development of reefs on structural blocks and close association with fluvial clastics. After Purser et al. (1987).

pelagické - CCD

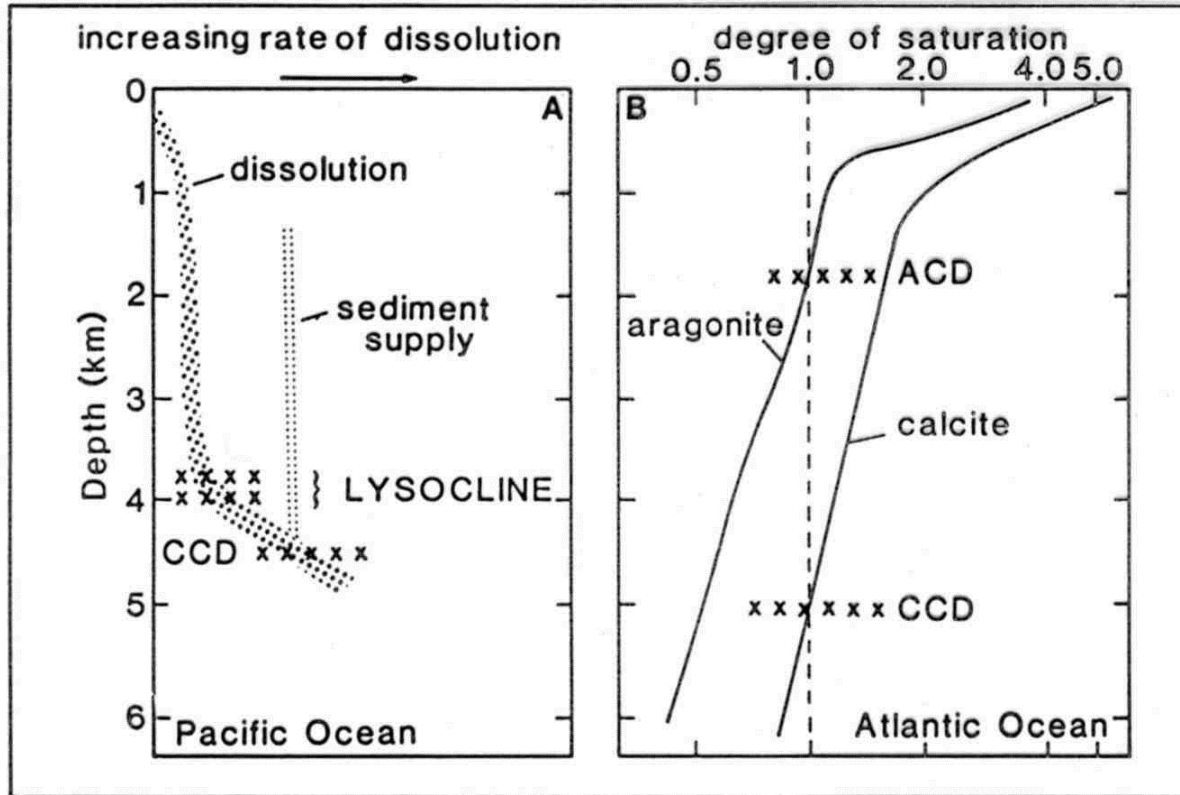


Fig. 5.1 Carbonate saturation and dissolution in the deep sea. (A) The profile of increasing CaCO_3 dissolution with increasing depth for the Pacific Ocean. The lysocline is the depth where the rate of dissolution increases markedly, and the CCD is the depth where the rate of sediment supply is matched by the rate of dissolution and below which therefore the sediments are CaCO_3 -free. After Jenkyns (1986). (B) The profiles of decreasing degree of saturation for aragonite and for calcite with increasing depth for the Atlantic Ocean. After Scholle et al. (1983).

cykličnost

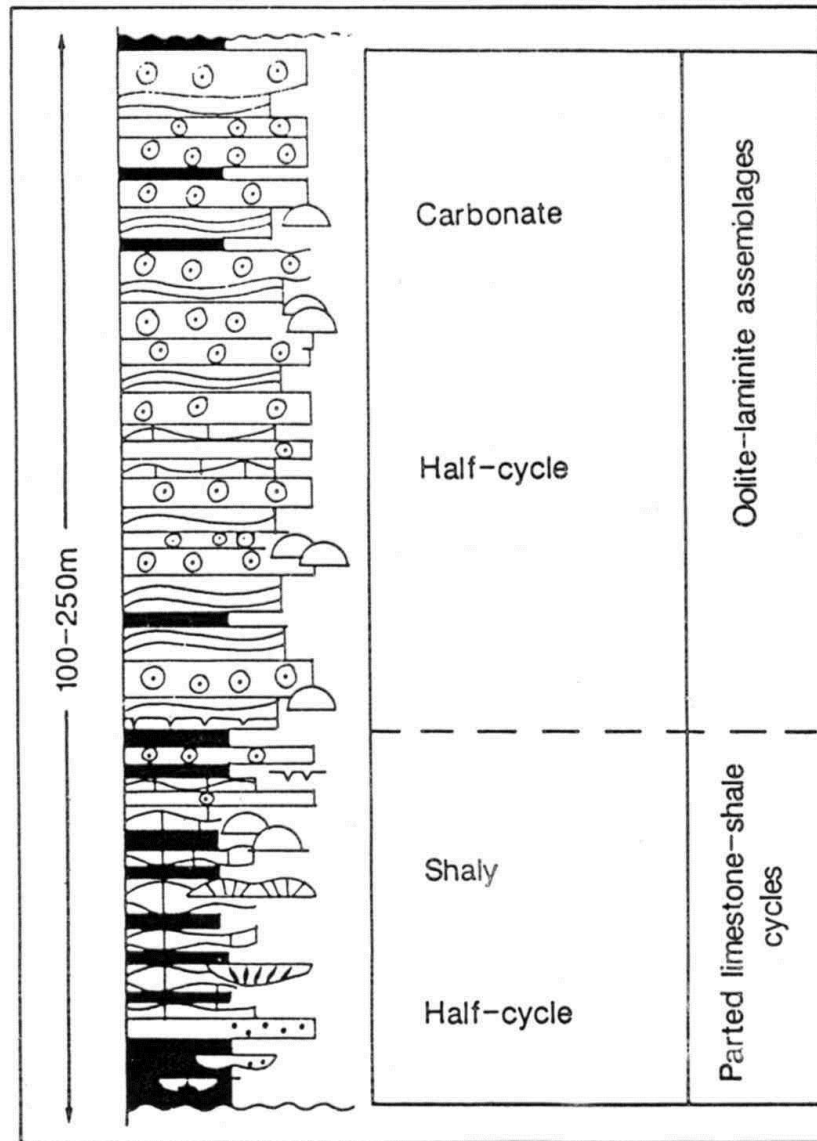
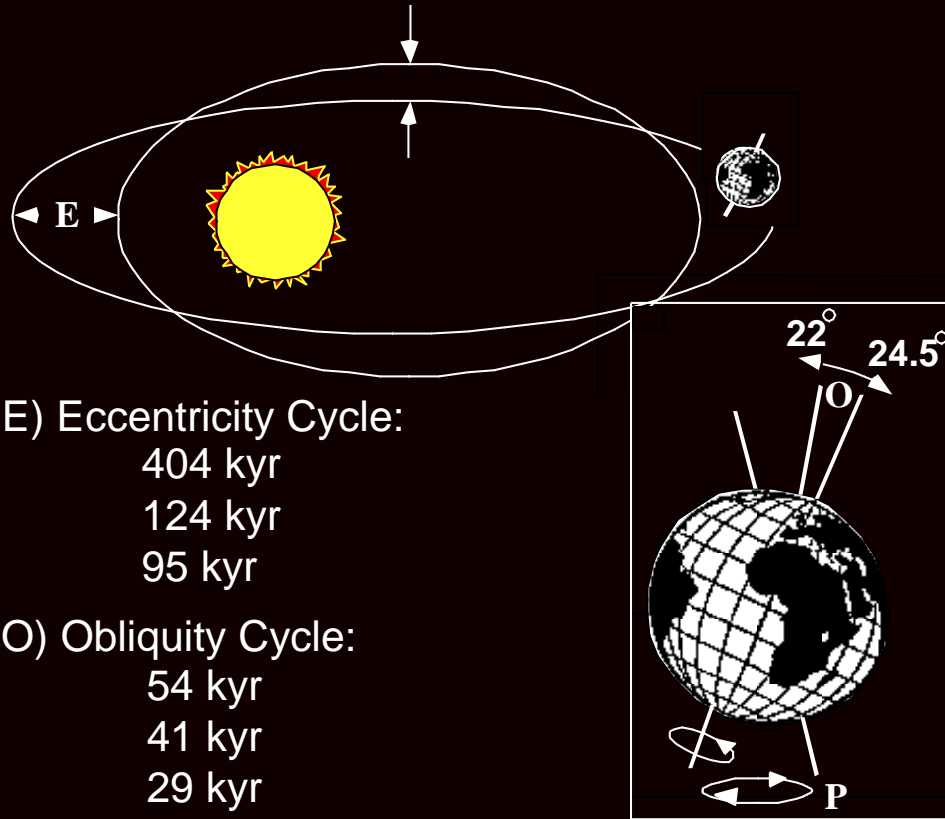


Fig. 2.29 Schematic Grand Cycle from the Cambrian of eastern North America consisting of many shale-limestone, shallowing-upward cycles in the lower part and oolite-stromatolite cycles in the upper part. After Chow & James (1987a).

Milankovitch Orbital Cyclicality



E) Eccentricity Cycle:
404 kyr
124 kyr
95 kyr

O) Obliquity Cycle:
54 kyr
41 kyr
29 kyr

P) Axial Precession Cycle:
23 kyr
19 kyr

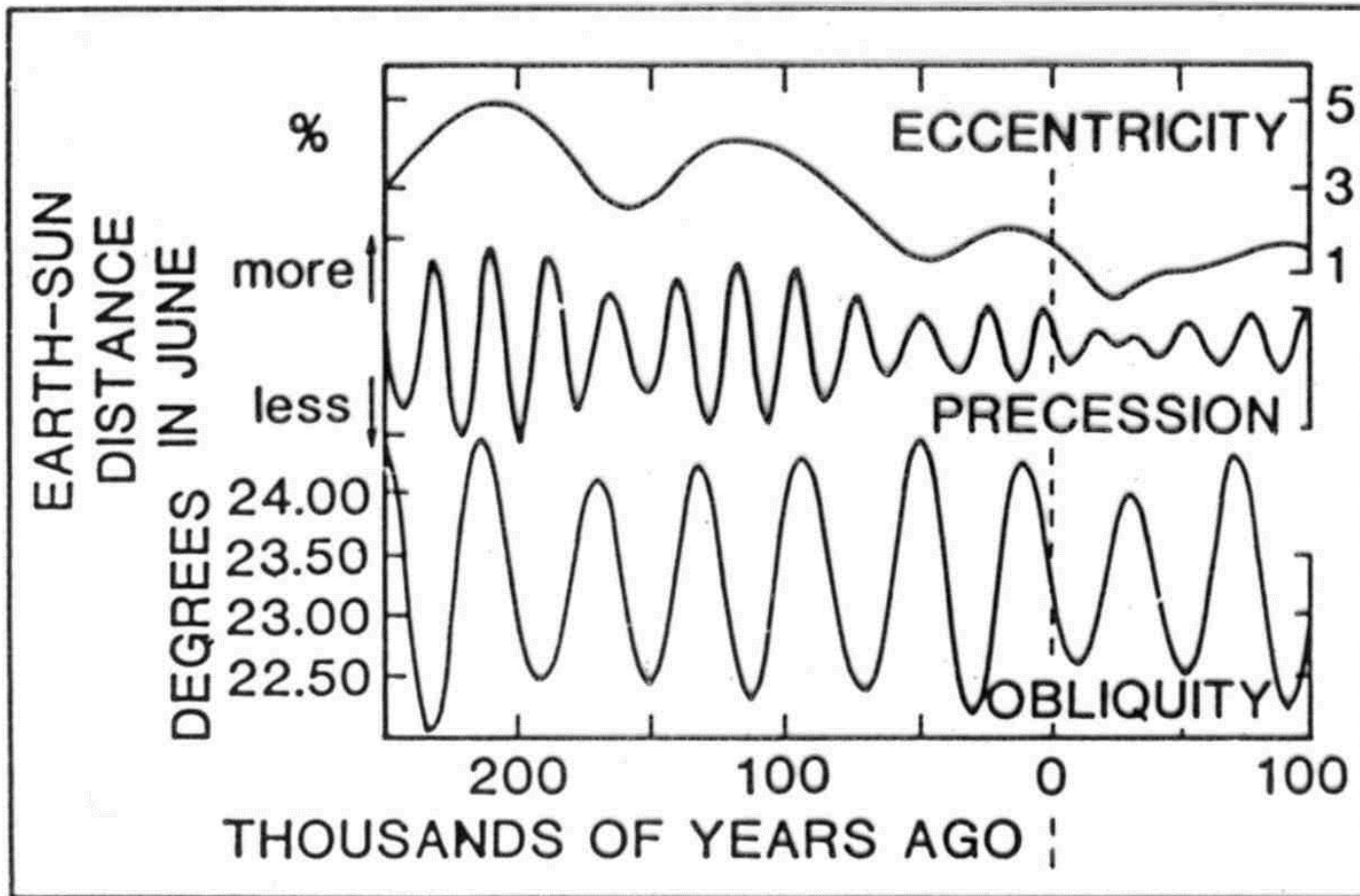
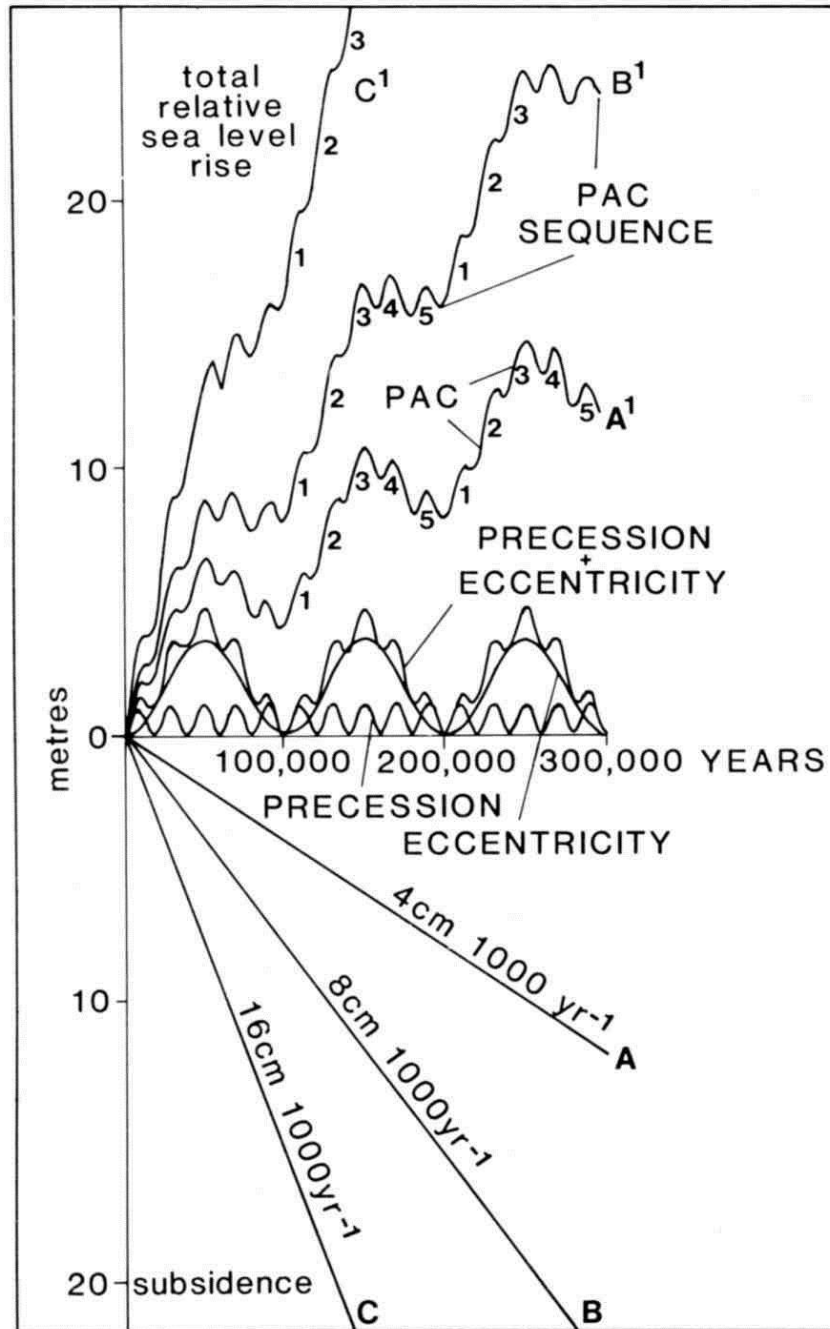


Fig. 2.30 *Milankovitch rhythms of the last 250 000 years, and into the future. After Imbrie & Imbrie (1980).*



čtení:

M.E.Tucker: Sedimentary petrology. 3rd ed. Blackwell, 2001(2003).

M.E.Tucker&V.P.Wright: Carbonate Sedimentology. Blackwell, 1994.

P.A.Scholle et al. (eds): Carbonate depositional environments. AAPG
Memoir 33, 1983.

Bathurst R.G.C. (1979): Carbonate sediments and their diagenesis.
Developments in sedimentology 12, Elsevier, Amsterdam.